UILU-ENG 86-3605

Report No. 128

OBSERVATIONS OF TENSION AND TORSION FATIGUE CRACKING BEHAVIOR AND THE EFFECT ON MULTIAXIAL DAMAGE CORRELATIONS

by

Julie Ann Bannantine

Materials and Design Division
Department of Mechanical and Industrial Engineering

A Report of the

MATERIALS ENGINEERING - MECHANICAL BEHAVIOR

College of Engineering, University of Illinois at Urbana-Champaign

July 1986

OBSERVATIONS OF TENSION AND TORSION FATIGUE CRACKING BEHAVIOR AND THE EFFECT ON MULTIAXIAL DAMAGE CORRELATIONS

ABSTRACT

A series of tension and torsion strain-controlled fatigue tests were conducted on several engineering materials. Detailed observations of nucleation and early crack growth were made. Cracking behavior is shown to depend upon loading mode (tension or torsion), strain amplitude and material type.

Three regions of cracking behavior were observed in torsion in AISI 304 and 316. In tests conducted at high shear strains, Region I, cracks initiated and remained on maximum shear strain (Stage I) planes. At intermediate strains, Region II, cracks initiated on shear planes but linked up to form growth on planes perpendicular to the maximum principal strain (Stage II). In Region III, at low strains, a few cracks initiated on shear planes but quickly branched and propagated on Stage II planes. Other materials exhibited characteristics of one or more of these regions when tested in torsion. Cracks in Inconel 718 remained on shear planes, Region I behavior, for a wide range of strain amplitudes while SAE 1045 exhibited Region II behavior only at very low strains. In gray cast iron, only tensile cracks, Region III behavior, were found.

Multiaxial models which were developed for shear strain dominated materials did not correlate multiaxial test results of a principal strain dominated material. Differences in cracking behavior for different materials and loading conditions need to be considered in successful life predictions for components subjected to multiaxial fatigue.

ACKNOWLEDGMENTS

This study was conducted in the Materials Engineering Research Laboratory at the University of Illinois at Urbana-Champaign and was supported by the Department of Energy Grant DE-AC02-76ER01198.

Professor Darrell F. Socie is acknowledged for the freedom to pursue and develop independent study as well as his insight and technical advice. Dr. Peter Kurath is acknowledged for his willing assistance and advice during the course of the work. Dr. Altstetter is acknowledged for his helpful advice and comments.

The author's family and friends are gratefully acknowledged for their constant encouragement. Finally, the author's husband, Sandy, is sincerely thanked for his patience, understanding, and unselfish support which have helped allow this work to be completed.

TABLE OF CONTENTS

LIST OF TABLES

LIST OF FIGURES

LIST OF SYMBOLS

a_1	Length of one of the two dominant tensile branch cracks
a_2	Shear crack length
a_3	Length of one of the two dominant tensile branch cracks
a_{SH}	Shear crack length
b	Fatigue strength exponent
c	Fatigue ductility exponent
E	Modulus of elasticity
G	Shear modulus
K,K'	Monotonic, cyclic strength coefficient
L	"As the crow flies" crack length
N	Number of cycles
$2N_f, N_f$	Number of reversals, cycles to failure
N_{SH}	Number of cycles spent in shear crack growth before bifurcation
n,n'	Monotonic, cyclic strain hardening exponent
R_ε	Ratio of maximum axial strain to minimum axial strain
R_γ	Ratio of maximum shear strain to minimum shear strain
α	Angle between the maximum principal strain and the plane normal to the specimen axis
$\hat{\gamma}$	Maximum shear strain amplitude
γ_f'	Shear fatigue ductility coefficient
γ_{max}	Maximum shear strain experienced during a complete load cycle
$\frac{\Delta\gamma}{2}$	Mid-surface shear strain amplitude
ε	Applied axial strain
$\bar{\varepsilon}$	Von Mises effective strain
$\hat{\varepsilon}_n$	Strain amplitude normal to the plane of maximum shear strain amplitude

ε_f'	Fatigue ductility coefficient
$\frac{\Delta\varepsilon}{2}$	Axial strain amplitude
$\frac{\Delta\varepsilon_1}{2}$	Maximum principal strain alternation
$\frac{\Delta\varepsilon^P}{2}$	Plastic axial strain amplitude
σ_f'	Fatigue strength coefficient
$\hat{\sigma}_{no}$	Mean stress normal to the plane of maximum shear strain amplitude
σ_1^{max}	Maximum normal stress on the plane experiencing the largest alternation of principal strain
$\frac{\Delta\sigma}{2}$	Axial stress amplitude
τ_f'	Shear fatigue strength coefficient
$\frac{\Delta\tau}{2}$	Shear stress amplitude

1. INTRODUCTION

The majority of fatigue research has been conducted under uniaxial loading conditions. To a lesser extent, work has been done in the area of torsional fatigue. In many applications, engineering components are subjected to complicated states of stress and strain. Successful multiaxial fatigue life predictions which are based upon physical observations require an understanding of the cracking behavior of materials. This research seeks to aid in the development of that understanding.

Cracking observations reported in the literature are reviewed. Results of tension and torsion strain controlled low cycle fatigue tests conducted on thin wall tubular specimens at room temperature are presented. Observations of nucleation and early crack growth are made for several engineering materials. Cracking behavior is observed to depend on loading mode (tension or torsion), strain amplitude, and material type. The impact on multiaxial theories is discussed.

2. BACKGROUND

Extensive research in uniaxial smooth specimen fatigue has shown that fatigue crack nucleation usually occurs at stress concentrations on or immediately below the surface of the material. These stress concentrations can result from surface roughness (due either to manufacturing or to intrusions and extrusions caused by cyclic slip), grain boundaries, or inclusions. Nucleation mechanisms vary for different materials.

Typically, ductile materials form slip bands. In 1902, Ewing and Humfrey [1] reported observations of slip bands in fatigue tests of Swedish iron. They initially observed formation of a few slip bands. As the test progressed, they observed an increased number with the earlier cited bands becoming broader and more distinct until cracks formed in the bands. These slip bands or planes, commonly referred to as persistent slip bands (PSBs), vary from the surrounding matrix by their dislocation structure [2-5]. Intrusions and extrusions associated with the PSBs are produced on the surface of the specimen. These tend to produce a notch effect and it is believed that this stress concentration causes cracking to occur in the PSBs.

Although this mechanism is the most general and widely observed, other modes of crack initiation exist. By varying alloying constituents or test conditions (i.e. very high strains [6]), fatigue cracks may be initiated at grain boundaries rather than from PSBs. In addition, PSBs are not observed in such materials as pure body-centered cubic (bcc) metals at low temperatures [4]. Inclusions may also influence fatigue crack initiation [7-8]. Fine and Ritchie [2] reported that in aluminum

alloys and high strength low alloy (HSLA) steels, inclusions aid in slip band fatigue crack initiation while cracked inclusions or debonding between inclusions and matrix were not observed.

Microstructure has a significant effect on crack initiation. Cold work, stacking fault energy, grain size, and alloying have all been shown to exhibit an influence. Crack initiation mechanisms have been widely discussed and reviewed [2-5,7,9].

The formation of PSBs first occurs, for most materials, in those grains whose slip planes are most closely aligned with the plane of maximum shear stress. Slip on these planes occurs as the result of the shear stress applied to the component. Gough [10] reported that crack nucleation is dependent upon the shear stress acting on the slip plane rather than the normal stress.

Forsyth designated crack initiation and growth on these planes as Stage I growth [11]. He reported that Stage I crack growth, which may dominate a significant portion of the fatigue life, continues until reversal of dislocation movement is prevented. The crack may then turn and propagate in a Stage II growth direction, on a plane normal to the maximum principal stress. This transition often occurs at grain boundaries [12,13]. Forsyth further reports that the criterion for Stage II growth is the value of the maximum principal tensile stress acting on the specimen in the region near the crack tip. When the ratio of shear stress to tensile stress reaches a critical value, the transition from Stage I to Stage II occurs.

As early as the 1920's, Gough [13] reported that shafts subjected to torsional fatigue fail in two general modes. In one mode, the crack

propagates axially or circumferentially. This corresponds to growth on the planes of maximum shear stress. In the second mode, the crack propagates on the planes of maximum principal stress which are 45 degrees to the axis of the shaft.

Materials that form slip bands in uniaxial fatigue also produce slip bands when tested in torsion. They occur on the planes of maximum shear (axial or circumferential directions for a tube or shaft). Peterson [14] observed that microcracks develop from these PSBs then grow in an axial, transverse (circumferential), or stepwise 45 degree direction. He reported, as did others, that harder materials tend to fail in the 45 degree or diagonal direction (plane normal to maximum principal stress) while ductile materials branch only at stress values not far above the endurance limit. Alternatively, Gough [20] believed it to be erroneous to make any such general statement. He believed 45 degree or spiral fractures were probably due to material inclusions or defects. Frost, March and Pook [7] also noted the tendency for harder materials to crack on tensile planes. They stated that obstacles to crack propagation such as intermetallics, flaws, and inclusions are much more likely to dominate in harder, more complex alloys. Cast iron is an example of a material with inherent flaws in the form of graphite flakes. Torsion tests of cast iron show 45 degree or tensile cracking at all strain levels.

One explanation [15,16] for the observed propensity of high hardness or brittle materials to fail in the tensile mode or 45 degree mode is related to the increase of shear strength and decrease in tensile strength with increasing hardness. The 45 degree failure occurs when

the tensile stress rises to the cohesive strength before the shear stress reaches the shear strength. This explanation is analogous to that used to account for differences in the monotonic torsion fracture modes of ductile and brittle materials.

Recently, increased research has been conducted in the area of torsional fatigue [17-21]. Hurd and Irving [17] observed a general dependency of cracking behavior on microstructure and strain amplitude for EN16 steel tempered to three strength levels. They noted that Mode III or shear cracks were most stable in the lowest strength steel, while the initiation of a 45 degree crack depended on the fatigue life. At high stress intensities, or shorter lives, the shear mode was favored. They also reported that induction hardening may improve fatigue lives of components subjected to torsional loading. The Mode I or 45 degree cracking is suppressed due to the compressive residual stresses developed during hardening.

Tschegg, Ritchie, and McClintock [19] observed that cracking behavior was dependent on microstructure and applied stress. Circular notched shafts made of AISI 4340 steel were subjected to torsional fatigue. Cracks were reported to initiate in a "macroscopically flat" manner in all specimens tested. At lower stress intensities and larger crack lengths, fracture surfaces developed into a local hill-and-valley morphology which they termed a "factory roof" fracture. This fracture mode was associated with Mode I, 45 degree branch cracks. Tschegg [20] postulated several reasons for this transition from Mode III, "macroscopically flat" fracture, to Mode I, "factory roof." These include mutual support of inclined surfaces, fretting fatigue, and mutual

support of debris. In AISI 4340 steel, Tschegg believed that the change of fracture mode was influenced by inclusions which act as initiation sites for the branch cracks in the plastic zone of the main crack.

These same authors observed a decrease in crack growth rate at constant values of stress intensity which was explained by an increase in roughness-induced crack closure. This is in agreement with the work of Hult [22], in 1958, who stated that the rate of growth will decrease due to the friction between crack surfaces. This friction is believed to reduce the stresses at the crack tip and consequently reduce growth rate.

In 1976, Parsons and Pascoe [12] reported observations of crack initiation and growth under biaxial stress for AISI 304 and QT35 steels using cruciform specimens. They observed two stages of cracking. In the primary stage, the more prominent surface cracks developed until displacements of the crack faces could be observed. The secondary stage then occurred with the linking of primary cracks.

In the pure shear condition, which is the strain state for torsion, Parsons and Pascoe reported that the primary and secondary cracks in QT35 were of a shear type. At high strains and later stages of propagation, they noted a transition to the tensile mode by linking of primary shear cracks. The AISI 304, at very high strains (above 2.5 percent), developed a large number of shear cracks which linked to form a tensile secondary crack. At strains between 1.13 and 2.5 percent, shear type primary and secondary cracks developed. Below strains of 1.13 percent, a transition from shear to tensile mode was observed. After this transition, four crack legs, which branched off the main

shear crack, continued to grow until failure. No secondary stage cracking was observed. Parsons and Pascoe believed shear cracking was favored at high strains due to a greater effect of crack tip plasticity and the large number of slip band cracks in neighboring grains.

Recently, several multiaxial theories have been developed [23-27]. Brown and Miller [23] proposed a theory which they reported was based upon physical crack observations. The primary damage parameter in this model for both Stage I and Stage II crack growth was the maximum shear strain. The tensile strain across the maximum shear strain plane was believed to have a secondary but important effect. Lohr and Ellison [24] later modified the theory based upon the premise that the shear strain on the plane growing into the thickness of the component was the most damaging. Jacquelin, Hourlier and Pineau [25] developed a multiaxial fatigue theory for Stage I crack initiation life based on results of stainless steel tests. They stated the belief that Stage I and Stage II behavior corresponds to two different physical processes and that it is important to distinguish between the two.

Although the importance of cracking behavior has been recognized, none of the multiaxial theories reviewed account for differences in this behavior. Instead, all material types and loading modes have been merged. Successful theories must correlate parameters with physically observed damage. Differences in crack behavior obviously will affect the importance of various parameters.

The purpose of this research was to study the effect of loading mode, strain amplitude, and material type on crack behavior and to evaluate the impact of the differences on multiaxial fatigue life predictions.

3. EXPERIMENTAL PROCEDURE

3.1 Testing Procedure

Strain controlled tension and torsion tests were conducted on thin-walled tubular specimens using internal extensometry and an automated servo-hydraulic, axial-torsional test system. The gauge section and internal diameter of all specimens was 25 mm. The wall thickness varied from 2 mm to 3.8 mm between materials. The monotonic tensile properties for four of the materials studied are given in Table 1.

3.2 Description of Materials

Stainless steel AISI 304 and AISI 316 tubular specimens were machined from hot rolled bar stock to a wall thickness of 3.8 mm. The chemical composition of the stainless steel materials are listed in Table 2. Baseline materials properties are listed in Tables 3 and 4.

The AISI 304 specimens were machined from two bars taken from the same heat of material. Chemistry and inclusion size remained essentially constant between the bars. Manganese sulfide stringers and spherical oxide inclusions were present in the AISI 304, the size and distribution of which were similar between bars. Figure 1 presents the results of an Auger analysis performed to identify the inclusions. The AISI 316 contained fewer inclusions, although the size was approximately the same as those in the AISI 304. The first bar of AISI 304, designated 304(A), had roughly a 20 μm grain size while the second bar of the 304, designated 304(B), and the AISI 316 both had a grain size of roughly 25 μm (Fig. 2). The smaller grain AISI 304 material, 304(A), achieved cyclically stable stresses up to 20 percent higher than the

AISI 304(B) material as shown in Table 5. Small tensile specimens were cut from the grip sections of tested AISI 304(A) and 304(B) tubular specimens. Monotonic tensile tests were conducted to verify baseline properties. Virtually no difference between the monotonic tensile properties of the two AISI 304 materials was observed.

Both the AISI 304 and 316 underwent a stress-induced phase transformation to martensite, although the amount of transformation was greater in the AISI 304. Two specimens were tested for martensite using a ferritescope. An AISI 304 specimen tested at 0.35 percent strain contained up to 6 percent martensite in the gauge section while the AISI 316 tested at 0.8 percent strain contained only up to 2 percent martensite.

The surfaces of failed AISI 304 specimens tested in torsion were lightly polished and etched to reveal crack interaction with microstructure. Several solid, 6.4 mm outside diameter, stainless steel 304 specimens were tested under axial strain controlled conditions. The fracture surface of these specimens was examined using scanning electron microscopy.

Comparisons of AISI 304 and 316 results were made to other materials recently tested with similar specimen geometries and loading conditions. These materials, Inconel 718 [27], SAE 1045 [28], and gray cast iron [29], are briefly described below. A detailed description of each may be found in the respective references.

Inconel 718 specimens were cut from a forged ring purchased to Aerospace Material Specification AMS 5663. The wall thickness was 2 mm and the grain size ranged from 20 to 100 μm. The SAE 1045, with a

specimen wall thickness of 2.5 mm, had a grain size of 35 to 40 μm and contained stringers of manganese sulfide inclusions. The gray cast iron, which was cast using a lost foam process, had a wall thickness of 3 mm.

3.3 Replication Procedure

All specimen surfaces were polished to a 0.5 micron finish in order to reduce surface roughness and enable cracks to be detected clearly. Crack nucleation and growth was monitored using acetate replicas taken at 10 percent intervals of expected life. Final failure was defined as a 10 percent drop in the stable load. Replicas were examined under an optical microscope using transmitted light.

4. TEST RESULTS AND OBSERVATIONS

Three modes of cracking behavior were observed in torsion. These are shown schematically in Fig. 3. In Region I, cracks initiated and remained on planes of maximum shear. Cracks in Region II initiated on shear planes, but branched to grow on tensile planes or Stage II planes by the linking of previously initiated shear cracks. Region III crack behavior was characterized by an initial shear crack growth followed quickly by branching and crack propagation on Stage II planes. No major linking of Stage II cracks occurred in Region III.

In tension, final failure occurred on planes normal to the maximum principal stress. In terms of the three regions described above, only Regions II and III behavior were observed in the tensile loading case.

Observations of the four material types are presented separately below. General discussion and comparison of cracking behavior follows.

4.1 Stainless Steel AISI 304 and 316

Detailed observations of crack growth in torsion were made at four fully reversed shear strain amplitudes, 1.7, 0.8, 0.6, and 0.35 percent, in the AISI 304 and 316 stainless steels. Cracking at the largest strain amplitude was characterized by Region I behavior. Cracks initiated in slip bands and at grain boundaries. Once initiated, the cracks become more distinct but showed no significant increase in length. At failure, a large density of small, coarse cracks dominated the surface of the specimen as shown in Fig. 4. A small amount of branching onto tensile planes (Stage II planes) was observed. However, the failure crack grew on the Stage I plane by a slow linking of previously initiated shear cracks.

Cracking behavior at 0.8 percent strain was characteristic of Region II. Cracks again initiated in slip bands and at grain boundaries. Bifurcation of Stage I cracks generally occurred at obstructions such as grain boundaries or triple points (Fig. 5). Again there was a large density of small cracks at failure as shown in Fig. 6. These cracks were longer and less coarse than the cracks developed in the specimens tested at 1.7 percent strain. Bifurcation or branching onto Stage II planes was observed for the vast majority of the microcracks. Growth of the main crack occurred on Stage II planes by a linking of previously initiated Stage I cracks such that the macroscopic growth occurred approximately 45 degrees to the axis of the specimen (Fig. 7).

Crack density was much smaller at 0.6 percent strain than that at 1.7 or 0.8 percent. Fine cracks, with a majority of Stage II growth, were observed on the specimen surface at failure as shown in Fig. 8. Cracks again branched at obstructions. Final failure occurred in a similar manner to the 0.8 percent test, i.e. Region II behavior.

Region III behavior was observed at the lowest strains. In general, the fraction of life spent growing the crack on shear planes was reduced as was the crack density. As shown in Fig. 9, the surface at failure was relatively free of microcracks. Rather, a small number of cracks initiated on shear planes but quickly branched to Stage II planes. Growth on these planes occurred by the propagation of the main crack rather than by a linking process (Fig. 10).

General cracking behavior and final failure was the same for both AISI 304 and 316. The difference in the cyclic stresses between the two

bars of AISI 304 affected the initiation and early growth of the Stage I cracks rather than overall crack characteristics. The material with the lower strength, AISI 304(B), exhibited shear or Stage I cracks which were longer and often initiated at inclusion sites. The shear cracks in the higher strength, AISI 304(A) were less than 0.1 mm for Regions II and III (Table 6). In the AISI 304(B) material, the shear cracks developed up to 2 mm for these same regions. In general, the fraction of life spent in shear growth increased with increasing strain amplitude (Fig. 11).

Some scatter in this trend of increased portions of life spent in shear growth with increased strain amplitude was due to the variation in inclusion size. Arrows in Fig. 11 indicate specimens which were particularly susceptible to inclusions. For example, a severe stringer, present in the AISI 316 specimen tested at 0.6 percent, caused a 4 mm shear crack to develop before it propagated in the Stage II direction (Fig. 12). This defect reduced the fraction of life spent developing the shear crack.

Surface replicas and scanning electron examination of fracture surfaces of the AISI 304 solid, 6.4 mm diameter, specimens tested in tension showed no perceptible evidence of Stage I growth. The fracture surface appeared to be almost entirely dominated by Stage II growth. It has been reported that at low strain amplitudes up to 90 percent of life may be taken up in initiation and Stage I growth, while at high strain amplitudes a similar fraction may be spent in Stage II crack growth [30].

4.2 Inconel 718

Unlike the stainless steel which displayed mixed behavior, results of the Inconel 718 tests showed that cracks initiate and remain on maximum shear planes, Region I behavior, at all values of shear strain. Torsion tests were conducted on the Inconel 718 at shear strain levels of 1.7, 0.8, 0.43, and 0.38 percent [31]. Even at the lowest strain amplitude, in which the strain was essentially all elastic, cracks initiated and remained on shear planes throughout the life. Figure 13A shows the failure crack developed in an Inconel specimen tested at 0.8 percent shear strain. As seen at failure, the crack never deviated from the plane of maximum shear.

Even under tensile loading, cracks remained on shear planes for the majority of fatigue life. Axial tests were conducted at two strain amplitudes, 1.0 and 0.5 percent. Final failure in all tension tests was in a macroscopic tensile direction comprised of large portions of microscopic shear growth. This is evident in Fig. 13A which shows the failure crack in a specimen tested in tension at 0.5 percent strain. Large amounts of shear growth are observed at failure. Growth on Stage II planes occurred only late in life.

Damage accumulation in Inconel appears to be shear dominated. This is attributed to the localized shear deformation bands developed during cyclic loading. The reversed movement of dislocations progressively shears the precipitates in these bands. Crack propagation then occurs along the bands with extensive shear crack growth exhibited throughout the fatigue life [32,33].

4.3 SAE 1045 Steel

Two types of cracking systems have been observed in SAE 1045 [28]. A large density of microcracks occurred at high amplitudes, with the final failure occurring by a very rapid linking of these cracks (Fig. 14). This type of damage has been termed the R system [34]. Alternatively, the S system [34], which dominated crack behavior at low strain amplitudes, exhibited one dominant crack which grew until failure (Fig. 15).

In torsion, at high amplitudes, the R system crack behavior was characteristic of Region I. The failure was similar to that observed in the stainless steels at high amplitudes except that the linking of microcracks and final failure in 1045 occurred over a very few cycles, while the growth of the Region I failure crack in stainless steels occurred progressively throughout the life. At lower amplitudes, progressive growth of a single crack (S system) occurred by a linking process on the shear plane. Both R and S type crack systems resulted in Region I behavior.

Region II behavior was only observed at long lives. At the lowest strain amplitude, 0.26 percent, the crack branched and growth occurred on the tensile plane by a linking of previously initiated shear cracks. After a period of tensile growth, the branch crack linked with a large shear crack which had been developing simultaneously. Final failure occurred by a mixture of Regions I and II behavior as shown in Fig. 16.

In tension, failure occurred in both the R and S systems on Stage II planes. Microcracks initiated on shear planes at high amplitudes,

1.0 percent strain, in a manner representative of the R crack system. A very rapid linking of these microcracks occurred immediately prior to failure such that the failure crack was on tensile (Stage II) planes. At low amplitudes, 0.2 percent, cracks initiated on shear planes but progressive growth occurred on Stage II planes as shown in Fig. 15.

4.4 Gray Cast Iron

In gray cast iron, cracks in tension and torsion propagated on Stage II planes at all strain levels [29]. Graphite flakes acted as small microcracks and linked to form growth on tensile planes. In torsion, after very few cycles at high shear strain amplitudes (0.6 percent), graphite flakes became very distinct. These continued to coarsen similar to the behavior of the Region I microcracks in stainless steel. However, unlike Region I behavior in stainless steel where microcracks linked on shear planes, in gray cast iron tensile (Stage II) cracks developed from the ends of the graphite flakes. These then linked up with cracks growing from other graphite flakes on tensile planes (Fig. 17). At low amplitudes, 0.2 percent shear strain, failure occurred by the same crack mechanism, although the number of cycles spent in the development and linking of cracks from the graphite flakes increased. Both tension and torsion at all amplitudes exhibited crack initiation from graphite flakes and subsequent growth on tensile planes with no significant shear growth.

5. DISCUSSION

Two types of cracking are generally observed in components subjected to fatigue--shear cracking associated with Stage I behavior and tensile cracking associated with Stage II behavior. Tension and torsion loading represent extreme cases for development of the two crack types. Crack observations made in tests conducted in tension and torsion show that cracking behavior is dependent upon loading mode, strain amplitude, and material type.

A major effect of loading mode on cracking direction is attributed to the normal strain on the plane of maximum shear (Fig. 18). As discussed previously, in tension, cracks generally initiate on shear planes but turn and propagate on planes perpendicular to the maximum principal stress or strain. The transition from shear growth to growth on tensile (Stage II) planes occurs primarily as a result of this normal strain across the maximum shear plane. In torsion, no normal strain exists on the maximum shear plane. This enables the shear (Stage I) crack to grow to a much greater length than the shear crack in tension.

Final failure in tension for all materials was characterized by macroscopic growth on Stage II planes. The fraction of fatigue life spent on Stage I planes varied with material and strain amplitude. Cracks in gray cast iron grew on tensile (Stage II) planes for virtually the entire life. Shear growth was eliminated as cracks originated at graphite flakes, which acted as microcracks, and grew on tensile planes. Stainless steels, tested in tension also exhibited little or no Stage I growth. Cracks in SAE 1045, tested at high tensile strain amplitudes (R crack system), initiated on shear planes. These cracks

coarsened until linking on Stage II planes occurred immediately prior to failure. At lower amplitudes (S crack system), cracks initiated on shear planes but quickly turned to Stage II planes. Lastly, Inconel crack behavior was characterized by a dominance of shear growth even in pure tension loading cases. Stage II growth occurred only late in life. Differences in crack behavior for each of the material types are summarized in Fig. 13. (In this figure, tension and torsion results for each material were compared individually at the same von Mises effective strain.)

Forsyth [11] suggested that the transition from Stage I to Stage II behavior occurs when the ratio of shear to tensile stress reaches a critical value. Although globally no normal or tensile strain occurs on the plane of maximum shear strain in torsion, tensile cracks developed in the stainless steels. Shear cracks often were observed to branch at grain boundaries or other obstructions. These obstructions may have caused a tensile strain to develop locally around the crack tip in torsion such that the crack branched to a tensile plane. In one stainless steel 304 specimen with a particularly large spherical inclusion, tested at an intermediate strain of 0.8 percent, a tensile crack initiated at a large spherical inclusion. It is probable that the tensile stress which developed locally around the inclusion caused growth to shift to the Stage II plane after a very short fraction of the life. An alternate source of local tensile stresses was presented by Tschegg [20]. He reported that the mutual support of inclined faces, or the rubbing between crack faces, may cause local tensile stresses to occur and therefore may explain the shift to tensile growth in materials tested in torsion.

The dependency of cracking behavior on strain amplitude is clearly evident from surface replicas of specimens tested in torsion. The planes of maximum shear, which are free of any normal strain, occur on the surface of the specimen rather than into the thickness. Surface observations allowed the strain amplitude dependency of Stage I and Stage II behavior to be closely monitored. From observations of stainless steel, a correlation between strain amplitude and cracking behavior was seen. In general, the fraction of life spent in shear growth decreased with a corresponding decrease in plastic strain.

Similar observations of the effect of plasticity were made by Tschegg, Ritchie and McClintock [19]. The "macroscopically flat" fracture which they observed at higher stress intensities corresponds to Region I behavior defined here. The "macroscopically flat" fracture followed by "factory roof" behavior corresponds to Region II behavior. In a later paper, they speculated that extensive plasticity was needed to sustain Mode III growth based upon the observation that Mode I or tensile growth occurs only at low stress intensities.

Parsons and Pascoe [12], who also observed crack branching in stainless steel AISI 304 at strains below 1.3 percent, postulated that shear cracking was favored at high strains due to a greater influence of crack tip plasticity and the large number of slip bands in neighboring grains. This explanation seems reasonable for materials which fail in shear modes at high values of plastic strain but branch to tensile planes at reduced strain amplitudes. Other factors must account for shear crack growth in materials, such as Inconel 718, in which crack growth remains on shear planes even at very low macroscopic plastic

strains. As discussed previously, In 718 develops localized shear deformation bands which cause extensive shear crack growth throughout the fatigue life, even at low values of plastic strain [33,34].

In addition to the effects of strain amplitude and loading mode, cracking behavior is largely influenced by material type. This is evident from the torsion tests results in which the materials were compared at similar ratios of plastic strain to total strain. At approximately equal values of elastic and plastic strain (50 percent ratio of plastic to total strain), AISI 304 and gray cast iron exhibited Region III behavior while crack behavior in SAE 1045 and Inconel 718 was characteristic of Region I (Fig. 19).

Observations further indicate that the ratio of plastic to total strain is not an appropriate parameter with which to characterize crack behavior. In Inconel 718, cracks remained on shear planes, Region I behavior, even at negligible macroscopic plastic strains. Conversely, even at very short lives, the cast iron failed on tensile planes. (This behavior in gray cast iron is explained by the presence of the graphite flakes which act as microscopic cracks.) In SAE 1045, Region II behavior was observed only at the lowest shear strain corresponding to a plastic to total strain ratio of 30 percent. Region II behavior was observed in AISI 304 at an 80 percent ratio of plastic to total strain. It is possible that materials which do not display Region II or III behavior in low cycle fatigue may exhibit behavior of these regions if tested at reduced plastic strains or very long lives. However, plastic strain values cannot be used for demarcation between the three regions.

It has been previously suggested that in torsion, ductile materials would fail on shear planes while brittle materials or those with inclusions, defects or other obstacles to crack propagation would fail on tensile planes. In contrast to this, the stainless steels and SAE 1045, which were both ductile and contained inclusions, did not fail in the same manner when tested in torsion at similar ratios of plastic to total strain.

Material type has a dominate influence on cracking behavior. Further research is required to explain variations of cracking behavior at constant values of plastic strain.

6. LIFE PREDICTIONS

Multiaxial fatigue theories should be based upon physically observed damage. None of the recently proposed strain based theories account for the differences in material cracking behavior observed in this study.

A modification to the theory of Brown and Miller has recently been proposed [27]. The parameter

$$\hat{\gamma} + \hat{\varepsilon}_n + \frac{\hat{\sigma}_{no}}{E}$$

in which $\hat{\gamma}$ is the maximum shear strain amplitude, $\hat{\varepsilon}_n$ is the strain amplitude normal to the plane of maximum shear strain amplitude, and $\hat{\sigma}_{no}$ is the mean stress normal to this same plane, accurately correlates the multiaxial fatigue test results of Inconel 718 (Fig. 20). As discussed previously and shown in Fig. 13A, damage accumulation in Inconel 718 was shear dominated. Even in tension, large portions of the fatigue life are spent in shear. It is to be expected that a shear based parameter would correlate results of a shear dominated material. For torsion tests, the parameter reduces to the shear strain amplitude. The solid line in Fig. 20 is the torsional strain life curve developed from torsion tests. The test results and model are described in detail in Ref. [31].

The same parameter was used to correlate results of multiaxial fatigue tests conducted using AISI 304 [35], a material which fails in a tensile mode. The predictions made using this parameter vary significantly from test results and are often nonconservative by an

order of magnitude (Fig. 21). It is not surprising that the shear based parameter did not correlate test results for a material dominated by tensile cracking.

Another model must be used to correlate the AISI 304 results. Life predictions for the tensile crack dominated material displayed improved correlation when analyzed with a combined principal stress-strain parameter

$$\frac{\Delta\varepsilon_1}{2}\,\sigma_1^{max}$$

developed by Smith, Watson, and Topper [36] for uniaxial tests. Implementation of this parameter for multiaxial fatigue is described in APPENDIX A. Failure occurred on tensile planes for all axial and multiaxial tests except for torsion tests at high shear strain amplitudes. In Fig. 22, the solid line was developed from axial test results. In the torsion tests conducted at high strain amplitudes, failure occurred on shear planes. It is not unexpected that these tests displayed the poorest correlation. The torsion tests at low strain amplitudes, where the failure crack developed on tensile planes, exhibited good correlation with the predictions.

Recognition of cracking characteristics is equally important when employing fracture mechanics analyses to predict fatigue life. Growth rates in Mode I have been shown to differ from Mode II and III rates [17]. Accurate life predictions will require an understanding of cracking behavior before correct stress intensity factors can be chosen for use in growth rate models.

Thus, it appears that successful fatigue life predictions, using either fracture mechanics concepts or strain-based multiaxial theories, will require careful considerations of cracking behavior of the material in question.

7. CONCLUSIONS

1. Fatigue cracking behavior is dependent upon loading mode, strain amplitude, and material type.
2. Three regions of crack behavior were observed in stainless steel AISI 304 and 316 tested in torsion. At decreasing plastic strains, there was a larger propensity for tensile growth. Many materials may exhibit these three regions if tested at sufficiently long lives in torsion.
3. Cracking behavior of different material types varies at a constant ratio of plastic to total strain. Plastic strain alone cannot be used to predict crack behavior for different material types.
4. A multiaxial fatigue model developed from test results of a material that fails in shear mode does not correlate multiaxial test results of a tensile crack dominated material. A maximum principal stress-strain parameter was successfully used to correlate results of the material which fails in a tensile mode.
5. Differences in cracking behavior for different materials and loading conditions will need to be considered in successful life predictions for components subjected to multiaxial fatigue.

TABLES

Table 1

Mechanical Properties of AISI 304 and 316,
SAE 1045, and Inconel 718

	0.2% Offset Yield Strength	Fracture Strength	Fracture Strain	Reduction in Area (%)
AISI 304	325 MPa	650 MPa	1.61	80%
AISI 316	555 MPa	725 MPa	1.73	82%
SAE 1045	380 MPa	985 MPa	0.71	50%
Inconel 718	1,160 MPa	1,850 MPa	0.33	28%

Table 2

Chemical Composition of Stainless Steel AISI 304 and 316

Element	AISI 304 (A)	AISI 304 (B)	AISI 316
Chromium	18.3	19.2	16.7
Nickel	9.3	10.8	12.1
Manganese	1.7	1.6	1.8
Silicon	0.52	0.40	0.55
Phosphorus	0.02	<0.01	0.01
Carbon	0.057	0.057	0.040
Sulfur	0.023	0.023	0.014

Results are reported in percent by weight.

< = less than

Table 3

Stainless Steel 304
Material Properties

MONOTONIC TENSILE PROPERTIES

E,	Elastic Modulus	183 GPa
σ_y2%,	0.2% Offset Yield Strength	325 MPa
σ_u,	Ultimate Strength	650 MPa
σ_f,	True Fracture Strength	1400 MPa
ε_f,	True Fracture Strain	1.731
% RA,	% Reduction in Area	80%
K,	Strength Coefficient	1210 MPa
n,	Strain Hardening Exponent	0.193

AXIAL CYCLIC PROPERTIES (R_ε = -1)*

E,	Elastic Modulus	185 GPa
σ_f'	Fatigue Strength Coefficient	1000 MPa
b	Fatigue Strength Exponent	-0.114
ε_f'	Fatigue Ductility Coefficient	0.171
c	Fatigue Ductility Exponent	-0.402
K'	Cyclic Strength Coefficient	1660 MPa
n'	Cyclic Strain Hardening Exponent	0.287

TORSIONAL CYCLIC PROPERTIES (R_γ = -1)**

G,	Torsional Modulus	82.8 GPa
τ_f',	Fatigue Strength Coefficient	709 MPa
b	Fatigue Strength Exponent	-0.121
γ_f',	Fatigue Ductility Coefficient	0.413
c,	Fatigue Ductility Exponent	-0.353
K',	Cyclic Strength Coefficient	785 MPa
n',	Cyclic Strain Hardening Exponent	0.296

* Axial properties obtained from tests using 304(B) material
** Torsional properties obtained from combined test results of 304(A) and 304(B) materials

Table 4
Stainless Steel 316
Material Properties

MONOTONIC TENSILE PROPERTIES

E,	Elastic Modulus	188 GPa
σ_y2%,	.2% Offset Yield Strength	555 MPa
σ_u,	Ultimate Strength	725 MPa
σ_f,	True Fracture Strength	2060 MPa
ε_f,	True Fracture Strain	1.73
%RA,	% Reduction in Area	82%
K	Strength Coefficient	1310 MPa
n,	Strength Exponent	0.14

TORSIONAL CYCLIC PROPERTIES (R_γ = -1)

G,	Torsional Modulus	76 GPa
τ_f',	Shear Fatigue Strength Coefficient	385 MPa
b,	Fatigue Strength Exponent	-0.05
γ_f',	Shear Fatigue Ductility Coefficient	1.11
c,	Fatigue Ductility Exponent	-0.49
K',	Cyclic Strength Coefficient	345 MPa
n',	Cyclic Strain Hardening Exponent	0.09

Table 5

Stainless Steel 304 and 316 Tubular Specimen Fatigue Data

Stainless Steel 304

(R = -1)

Specimen I.D.	Material Type	Loading Mode	$\Delta\gamma/2$	$\Delta\varepsilon/2$	$\Delta\tau/2$ (MPa)	$\Delta\sigma/2$ (MPa)	N_f (Cycles)
SS08	SS304(A)	Torsion	0.0173	0	248.2	0	4090
SS05	SS304(A)	"	0.0080	0	191.0	0	48,500
SS21	SS304(B)	"	0.0080	0	155.1	0	32,100
SS22	SS304(B)	"	0.0080	0	157.2	0	33,900
SS07	SS304(A)	"	0.0060	0	156.5	0	133,000
SS16	SS304(B)	"	0.0060	0	139.3	0	83,400
SS09	SS304(A)	"	0.0035	0	139.3	0	1.1×10^6
SS20	SS304(B)	"	0.0035	0	124.1	0	824,200
SS15	SS304(B)	Axial	0	0.0046	0	279.2	10,300
SS06	SS304(B)	Axial	0	0.0035	0	235.8	38,500

Stainless Steel 316

(R = -1)

Specimen I.D.	Material Type	Loading Mode	$\Delta\gamma/2$	$\Delta\varepsilon/2$	$\Delta\tau/2$ (MPa)	$\Delta\sigma/2$ (MPa)	N_f (Cycles)
SJ03	SS316	Torsion	0.0173	0	259.9	0	2,300
SJ01	SS316	"	0.0080	0	199.0	0	38,000
SJ02	SS316	"	0.0060	0	193.1	0	99,800
SJ07	SS316	"	0.0060	0	191.0	0	114,700
SJ04	SS316	"	0.0035	0	184.1	0	585,200
SJ08	SS316	"	0.0035	0	184.1	0	1,024,000
SJ06	SS316	"	0.0030	0	182.7	0	939,500
SJ05	SS316	Axial	0	0.0035	0	339.9	27,100

(All Stresses and Strains are Mid-Section Values)
(Tabulated Stresses are Cyclically Stable Values)

Table 6

Portion of Life Spent in Shear Crack Growth
and Length of Shear at Bifurcation
in AISI 304 and 316

TORSIONAL STRAIN LEVELS

Material	1.17% Spec. I.D.	N_f (Cycles)	$\frac{N_{SH}}{N_f}$	a_{SH} (mm)	0.8% Spec. I.D.	N_f (Cycles)	$\frac{N_{SH}}{N_f}$	a_{SH} (mm)
AISI 304(A)	SS08	4090	1.0	>10	SS05	48,000	0.19	0.1
AISI 304(B)					SS21	32,070	0.13	0.19
					SS22	33,900	~0*	2.2
AISI 316	SJ03	2320	1.0	>10	SJ01	38,000	0.66	1.2

Material	0.6% Spec. I.D.	N_f (Cycles)	$\frac{N_{SH}}{N_f}$	a_{SH} (mm)	0.35% Spec. I.D.	N_f (Cycles)	$\frac{N_{SH}}{N_f}$	a_{SH} (mm)
AISI 304(A)	SS07	133,150	0.08	0.1	SS09	1.17×10^6	~0	~0
AISI 304(B)	SS16	83,410	0.36	2.0	SS20	824,170	0.24	0.2
AISI 316	SJ02	99,810	0.40	1.0	SJ04	585,240	0.27	1.6
	SJ07	114,730	0.17	4.0	SJ08	1.02×10^6	0.25	0.12

* Particularly Severe Inclusion

Table 7

Stainless Steel 304

Smooth Specimen Fatigue Data

(R = -1)

Specimen I.D.	$\Delta\varepsilon/2$	$\Delta\varepsilon^P/2$ (Cycles)	$\Delta\sigma/2$ (MPa)	σ_o (MPa)	N_f (Cycles)
S-03	0.0100	0.0080	383	2.0	1,070
S-09	0.0100	0.0078	426	-1.4	1,170
S-06	0.006	0.0038	379	-21.9	6,080
S-01	0.0035	0.0021	261	5.8	30,700
S-10	0.0035	0.0021	258	-9.1	33,600
S-11	0.0035	0.0021	266	8.4	28,990
S-12	0.002	0.0008	230	16.5	286,390
S-02	0.002	0.0008	206	2.9	333,110

FIGURES

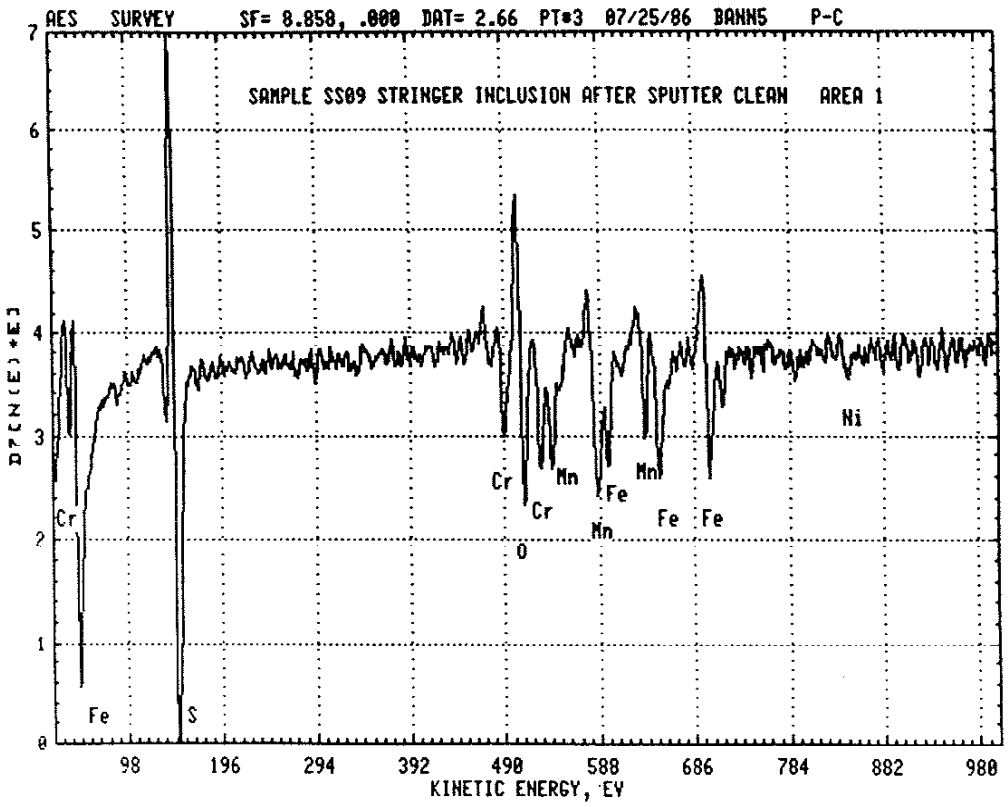

Figure 1A Results of Auger Analysis Performed on Manganese Sulfide Stringers Inclusions in AISI 304

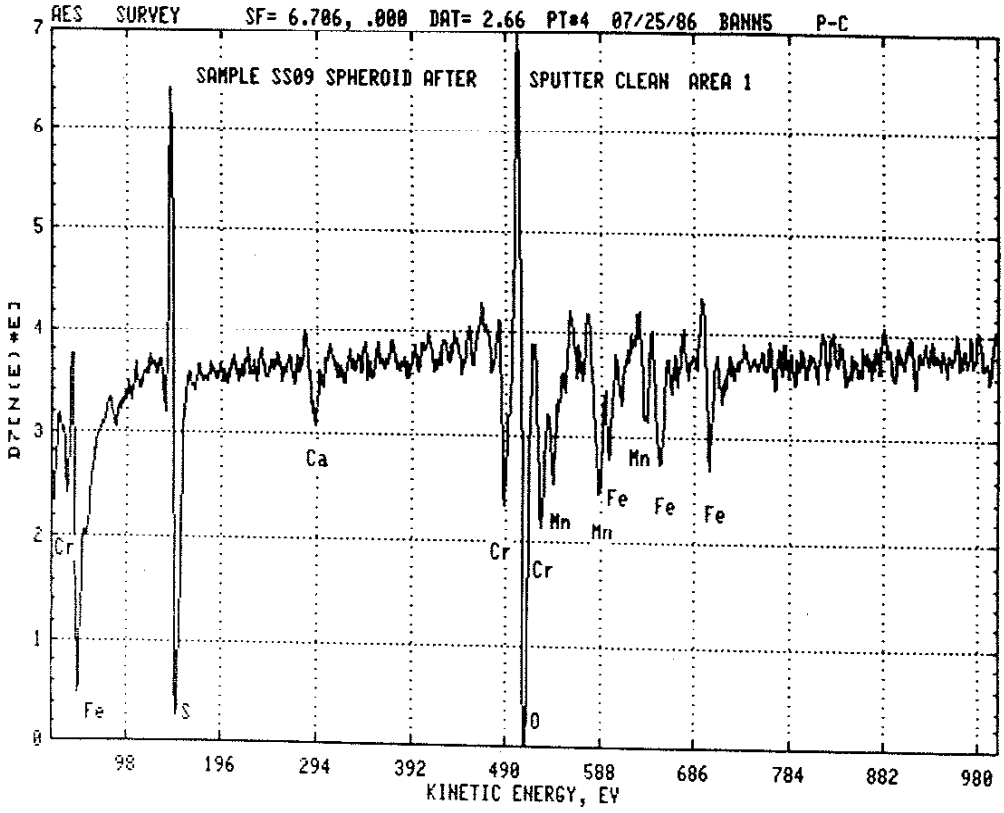

Figure 1B Results of Auger Analysis Performed on Spherical Oxide Inclusions in AISI 304

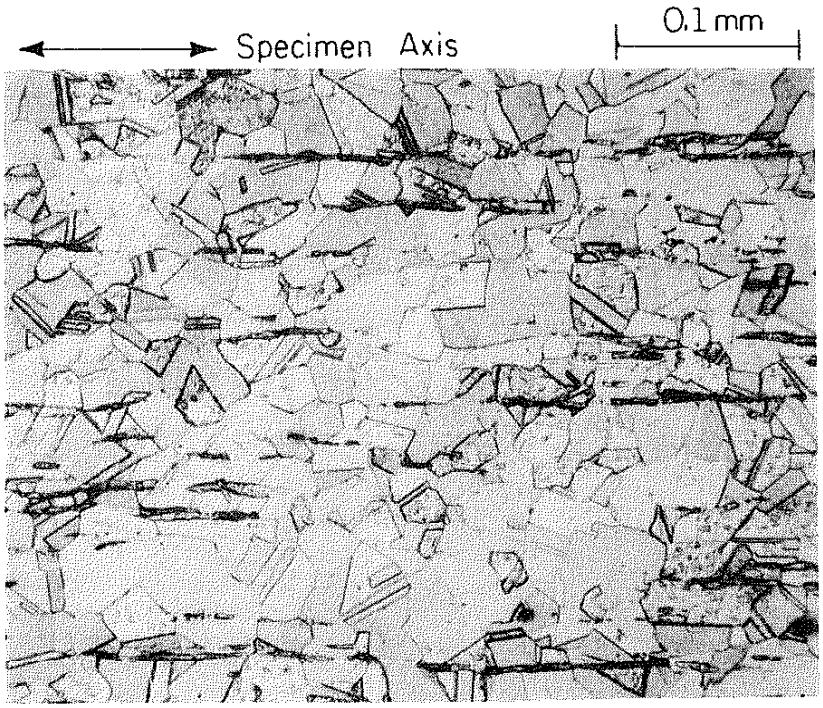

Figure 2A Microstructure of AISI SS304(A) ~ 20μm Grain Size

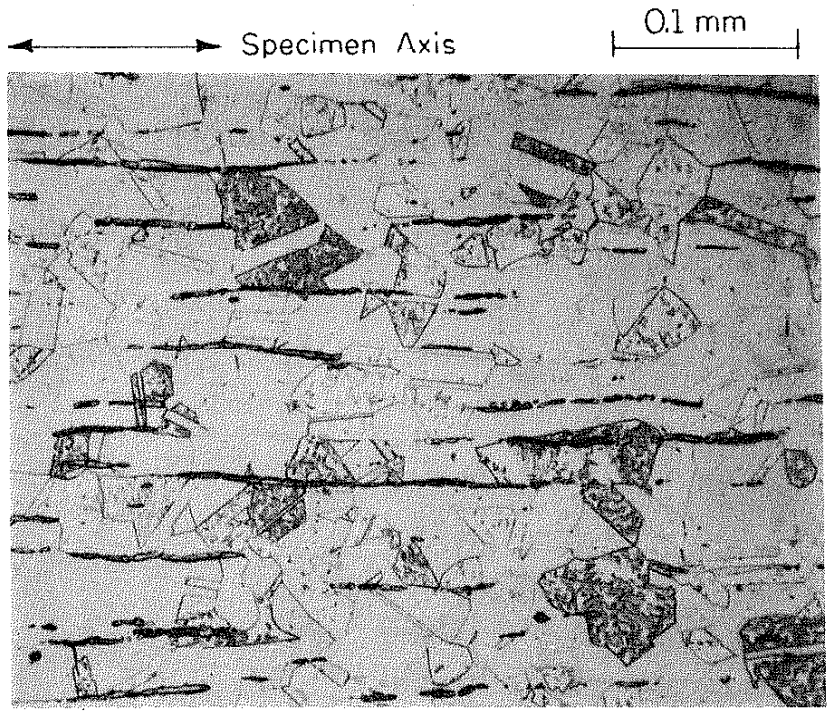

Figure 2B Microstructure of AISI SS304(B) ~25μm Grain Size

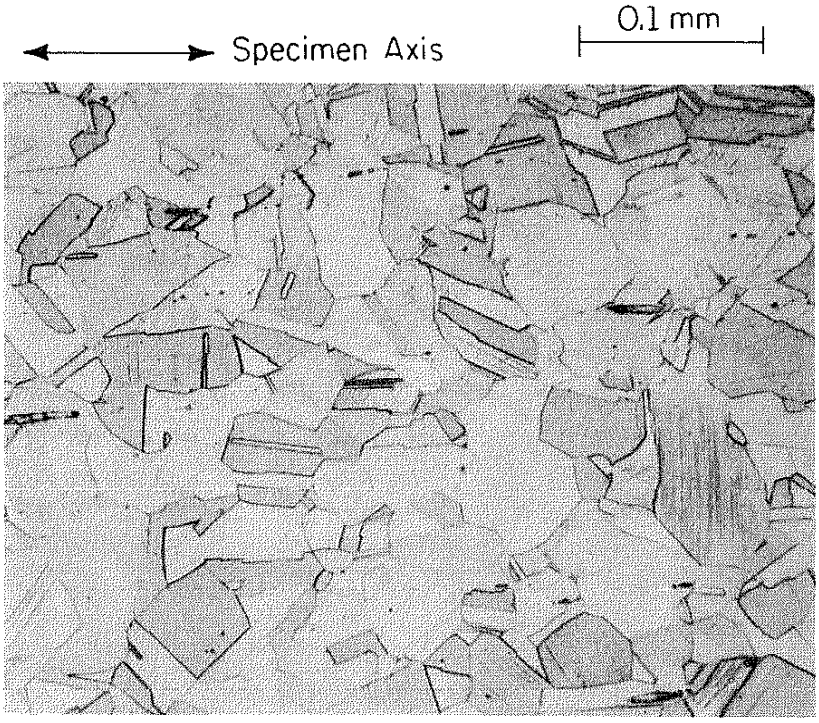

Figure 2C Microstructure of AISI 316 ~25μm Grain Size

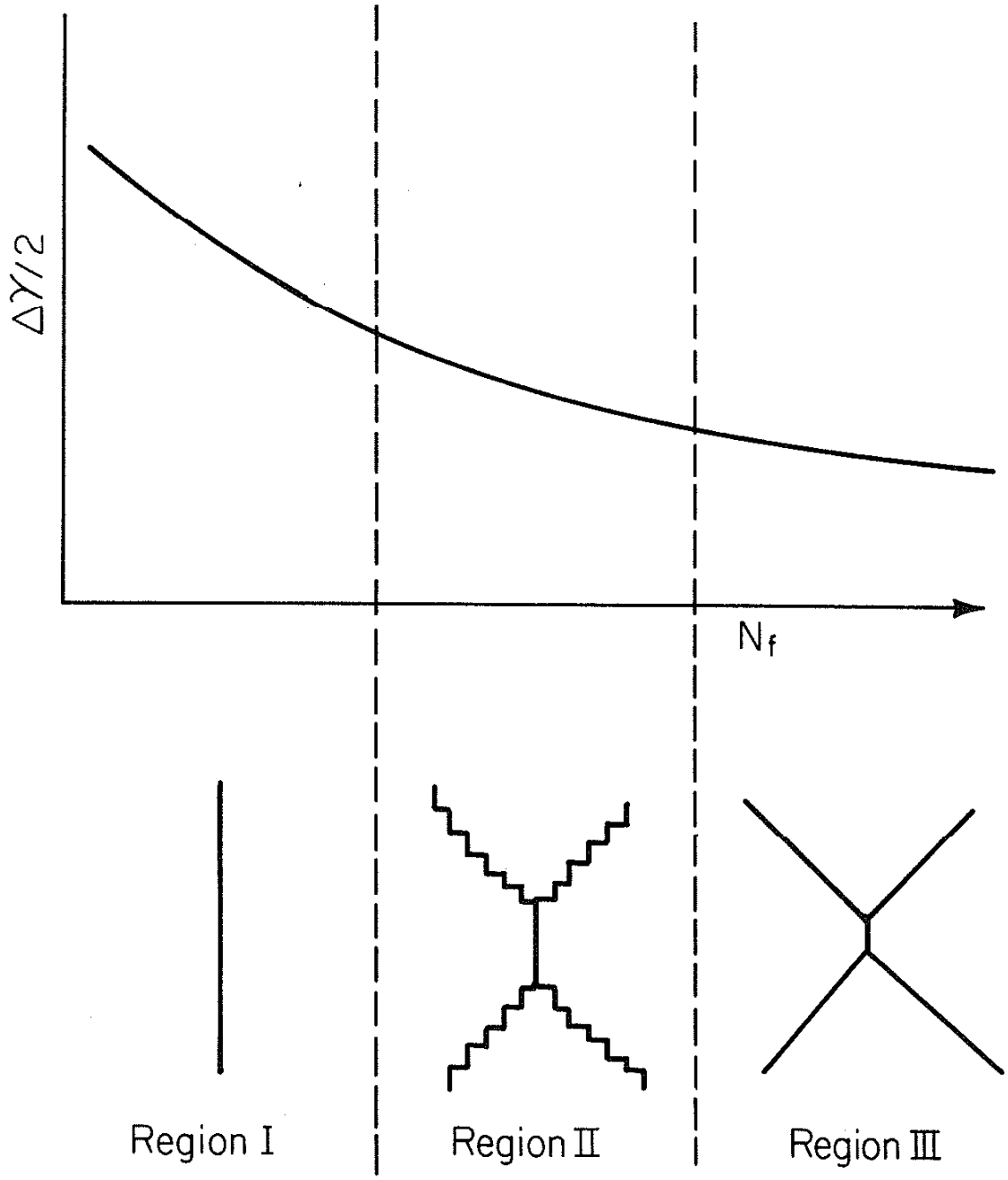

Three Regions of Cracking Behavior Observed in Torsion

Figure 3

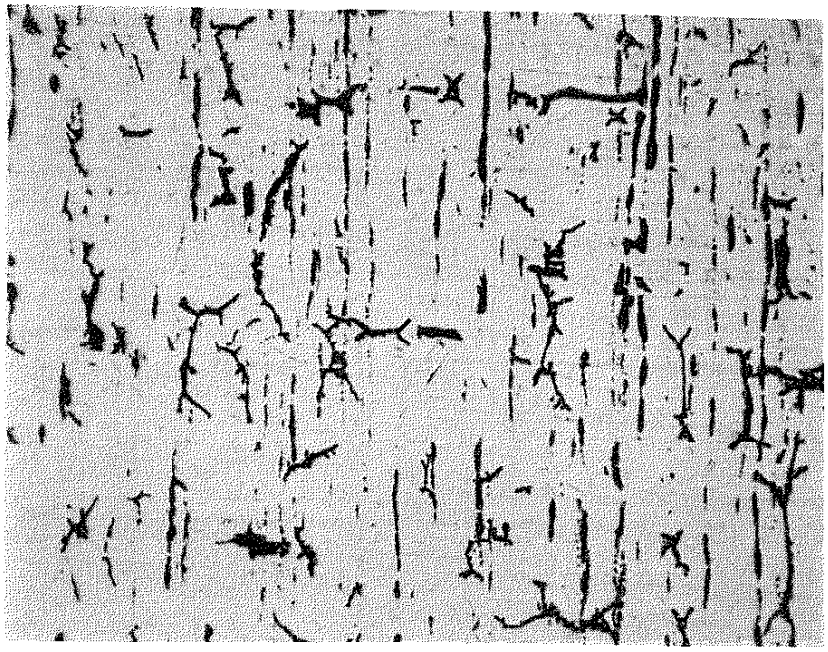

SPECIMEN AXIS

0.1mm

$\frac{\Delta\gamma}{2} = 1.7\%$ $N = N_f = 4090$

STAINLESS STEEL AISI 304 (SS08)
SPECIMEN SURFACE AT FAILURE
MICROCRACKS & STRINGER INCLUSIONS
VISIBLE.

Figure 4

SPECIMEN AXIS 0.1mm $\frac{\Delta\gamma}{2} = 0.8\%$ $N = N_f = 48{,}500$

STAINLESS STEEL A1S1 304 (SS05)
BIFURCATION OCCURS AT GRAIN BOUNDARIES

Figure 5

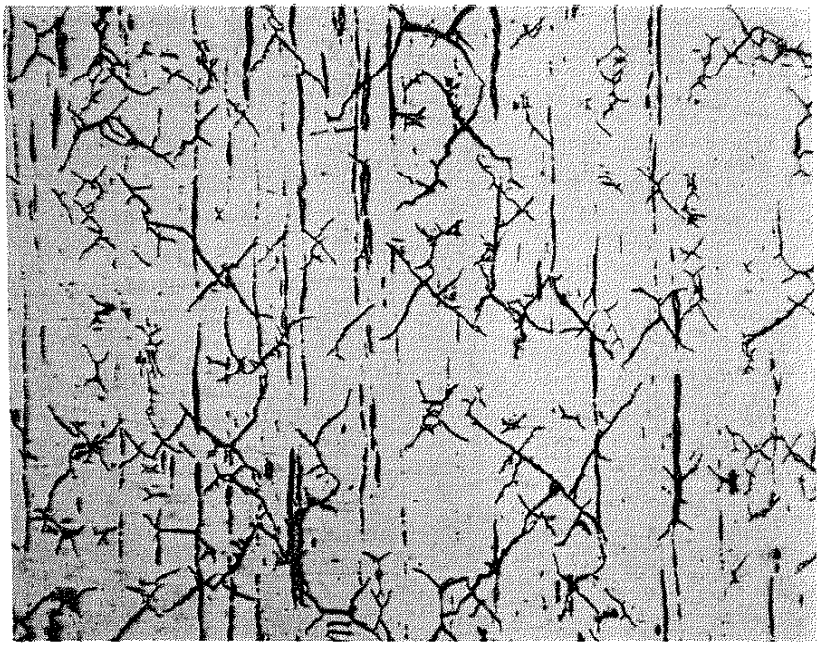

SPECIMEN AXIS

0.1mm

$\frac{\Delta\gamma}{2} = 0.8\%$ $N = N_f = 48{,}500$

STAINLESS STEEL A1S1 304 (SS05)
SPECIMEN SURFACE AT FAILURE

Figure 6

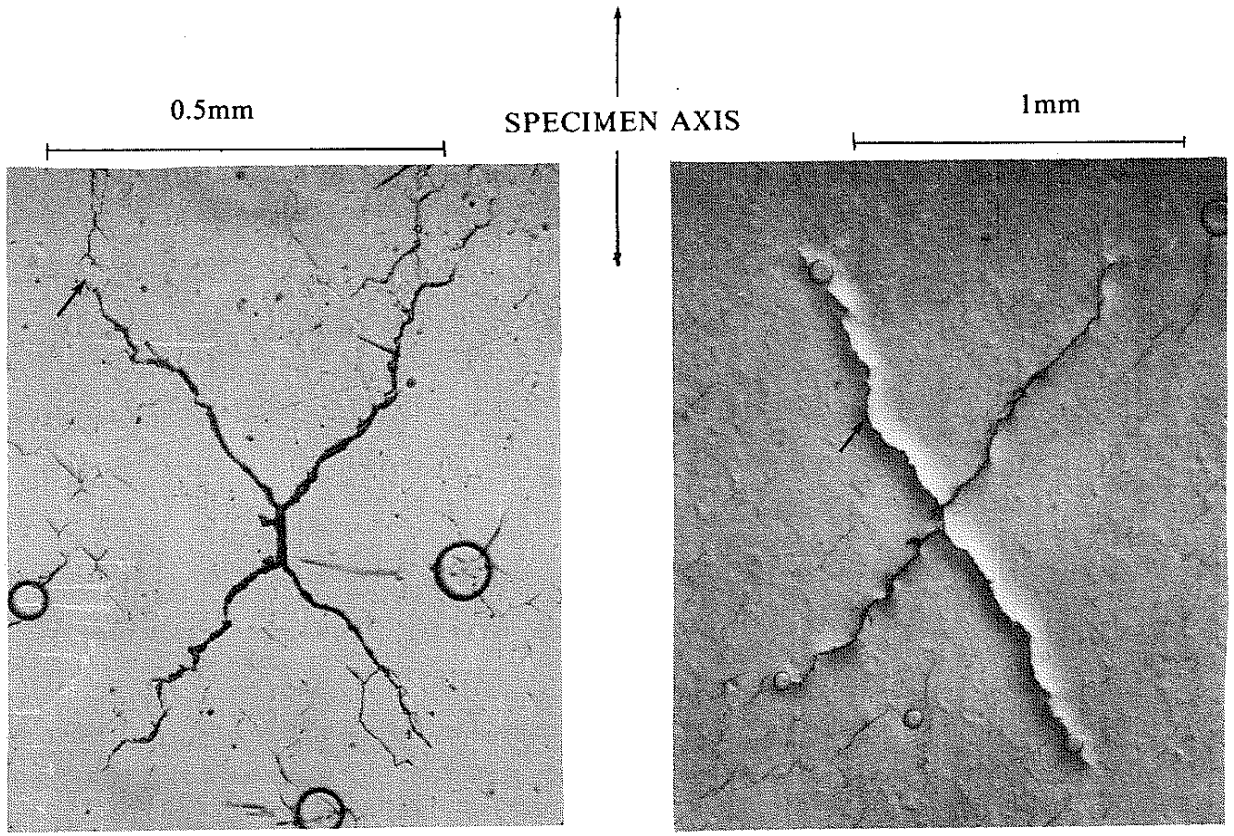

$$\frac{\Delta\gamma}{2} = 0.8\% \quad N_f = 48{,}500$$

STAINLESS STEEL AISI 304 SS05

Figure 7 Stainless Steel AISI 304 (SS05) Region II Behavior, Growth on Tensile Planes Occurs by Linking. (Arrows Indicate Same Location of Specimen)

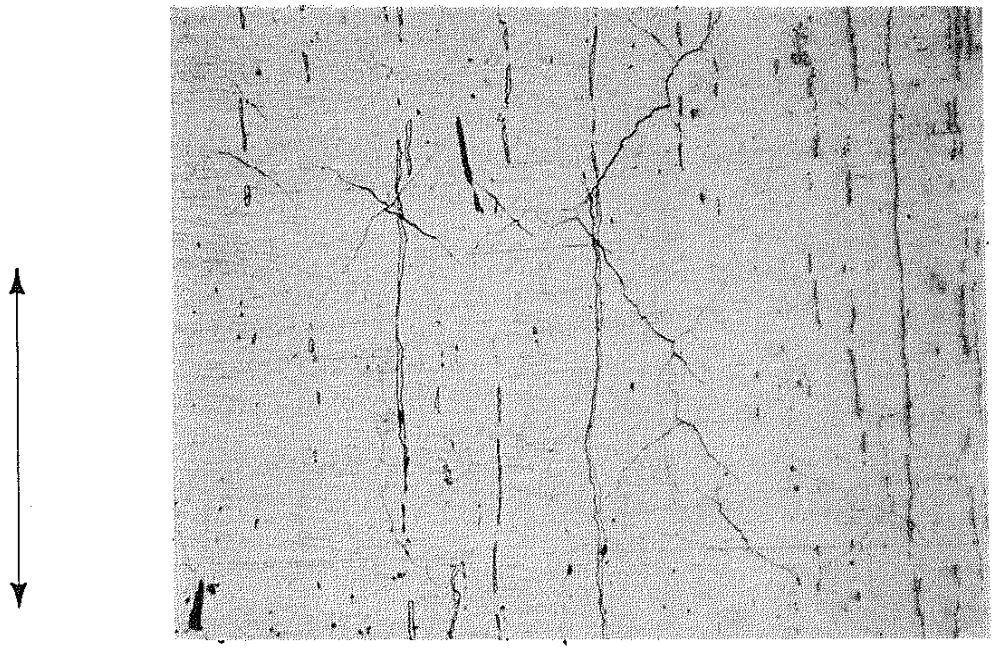

SPECIMEN AXIS 0.1mm $\frac{\Delta\gamma}{2} = 0.6\%$ $N = N_f = 133{,}000$

STAINLESS STEEL A1S1 304 (SS07)
SPECIMEN SURFACE AT FAILURE

Figure 8

SPECIMEN AXIS

0.1mm

$\frac{\Delta\gamma}{2} = 0.35\%$ $N = N_f = 1.1 \times 10^6$

STAINLESS STEEL AISI 304 (SS09)
SPECIMEN SURFACE AT FAILURE

Figure 9

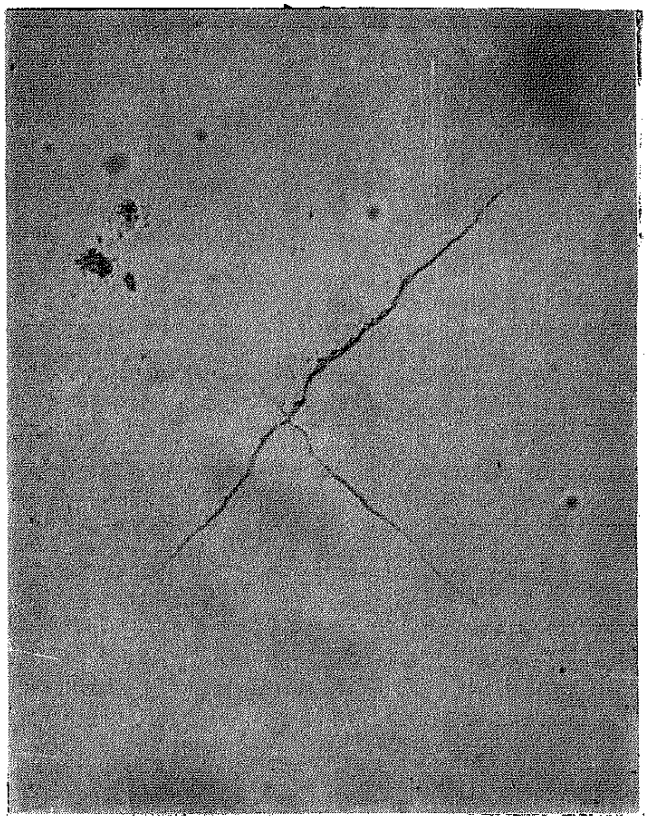

Figure 10 Stainless Steel AISI 304 (SS09) Region III Behavior. Growth on Tensile Planes Occurs by Propagation Rather than Linking

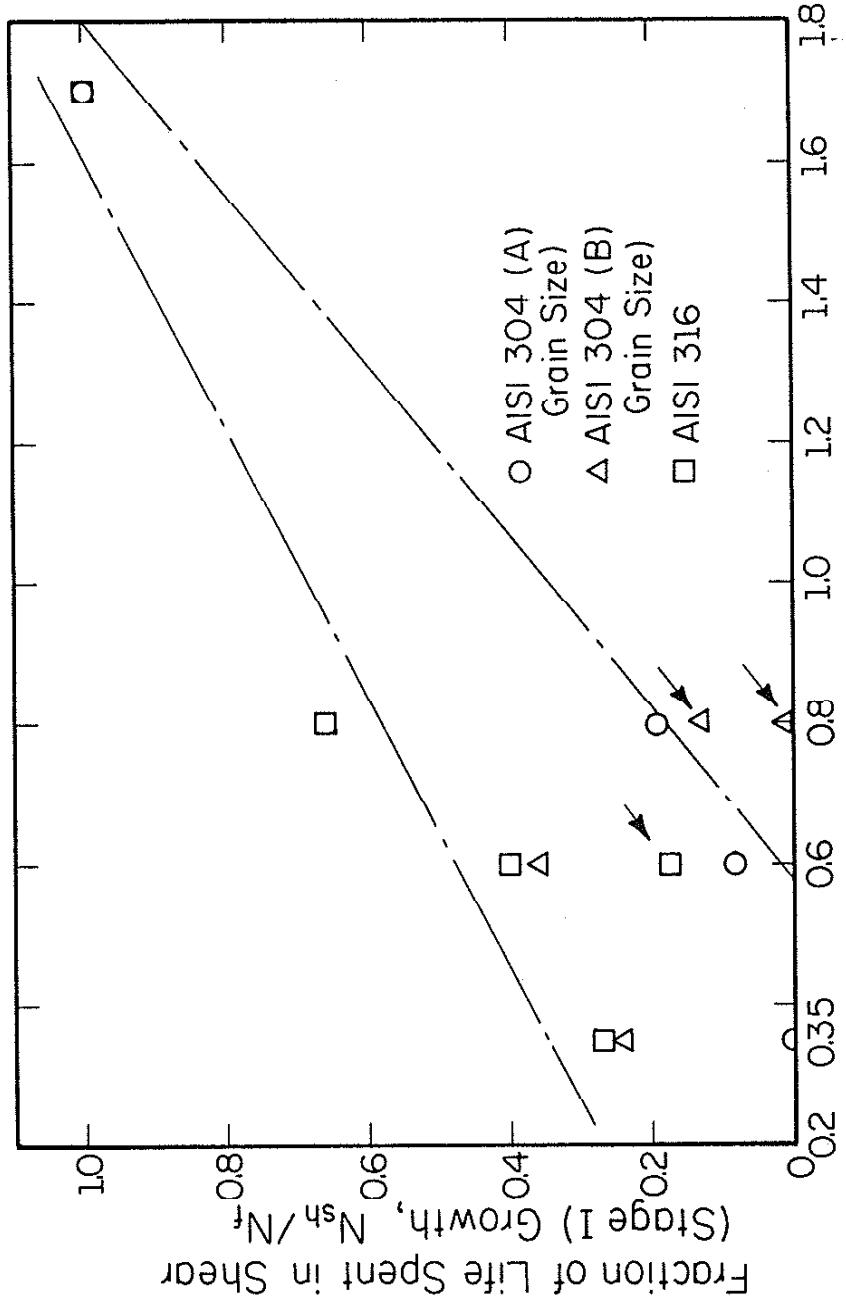

Fraction of Life Spent in Stage I Growth as a Function of Shear Strain Amplitude

Figure 11

SPECIMEN AXIS 0.1mm

$\frac{\Delta\gamma}{2} = 0.6\%$ N = 1,000

$N_f = 114{,}700$

STAINLESS STEEL A1S1 316 (SJ07)
SEVERE STRINGER INCLUSION VISIBLE. INITIAL SHEAR CRACKING OBSERVED AFTER 1000 CYCLES.

Figure 12

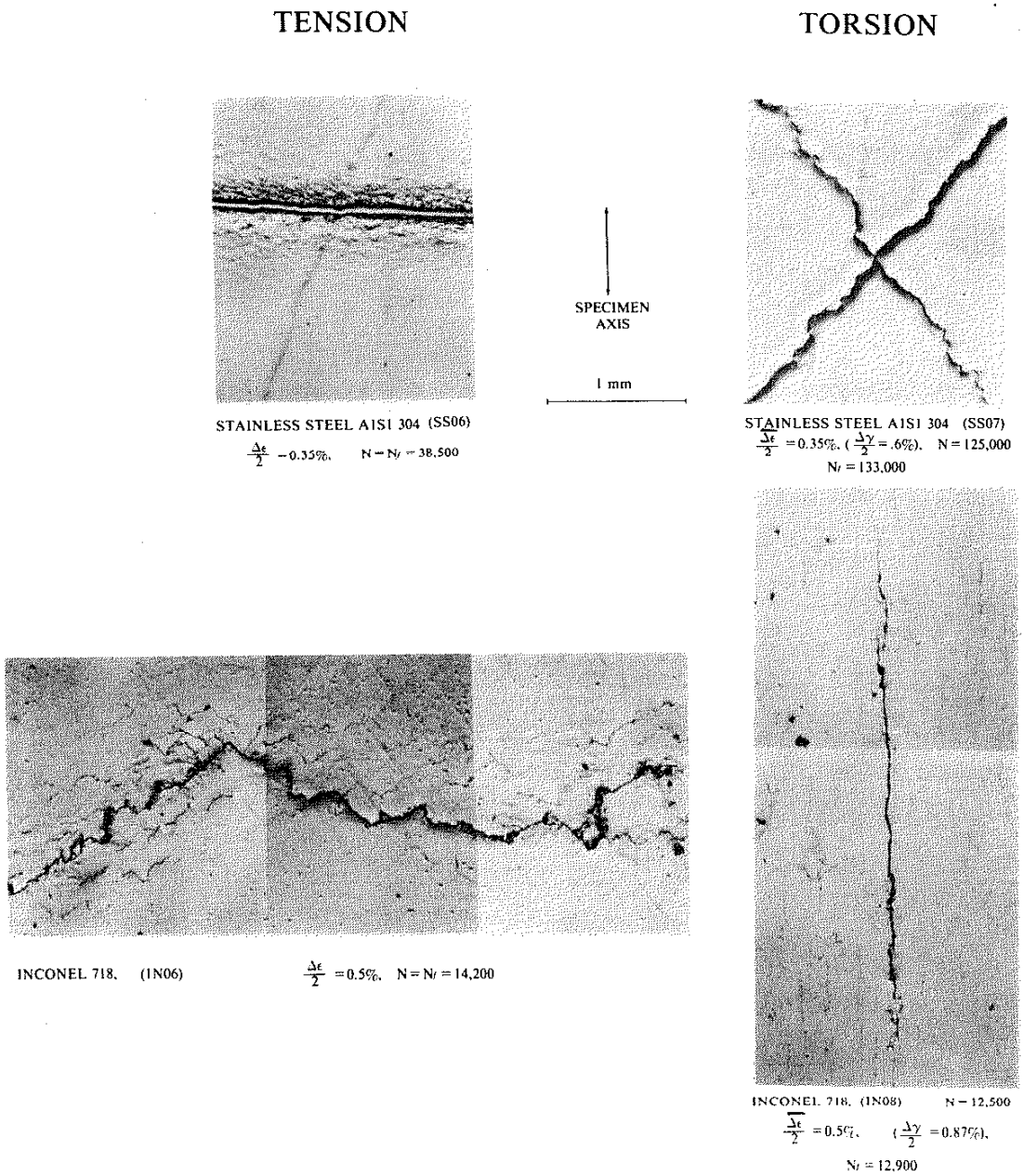

Figure 13A Tension and Torsion Behavior of AISI 304 at $\frac{\Delta\epsilon}{2}$ = 0.35%, and Inconel 718 at $\frac{\Delta\epsilon}{2}$ = 0.5%

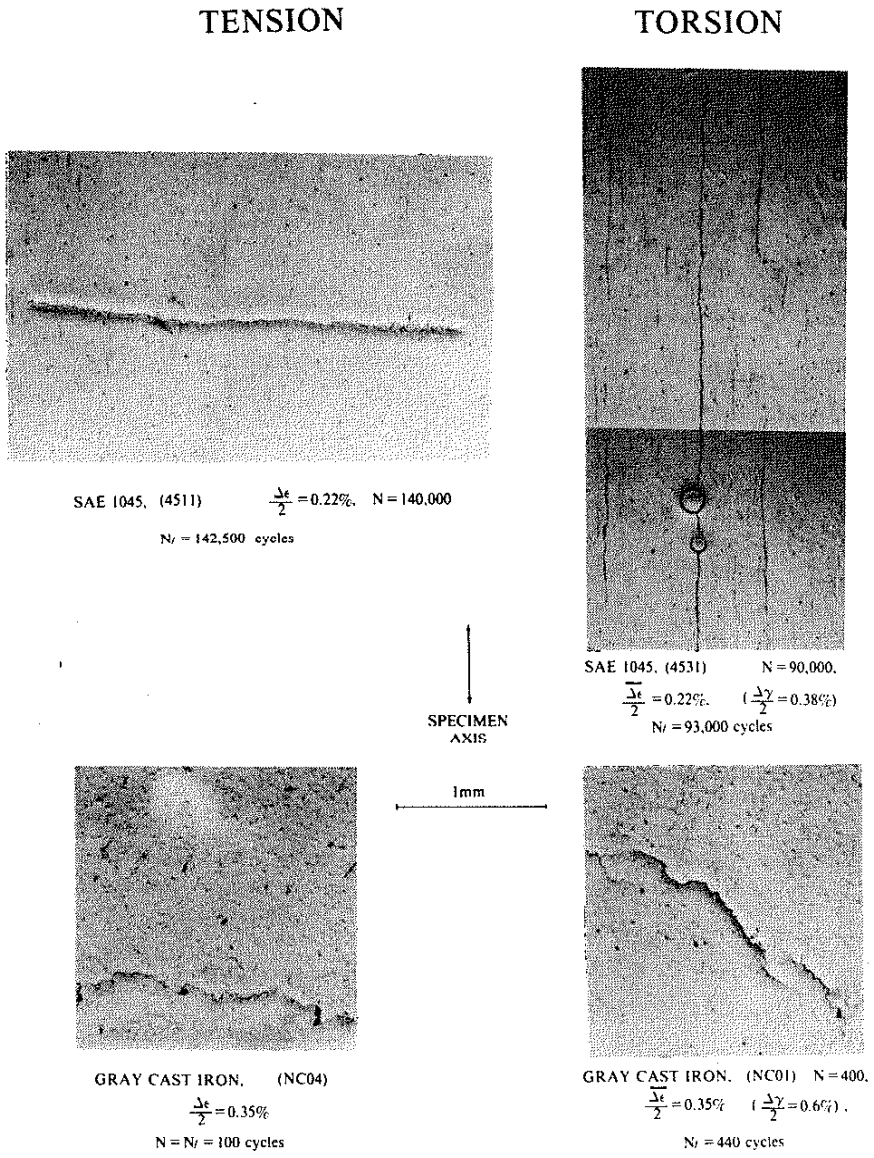

Figure 13B Tension and Torsion Behavior of SAE 1045 Steel at $\frac{\Delta\varepsilon}{2}$ = 0.22%, and Gray Cast Iron at $\frac{\Delta\varepsilon}{2}$ = 0.35%

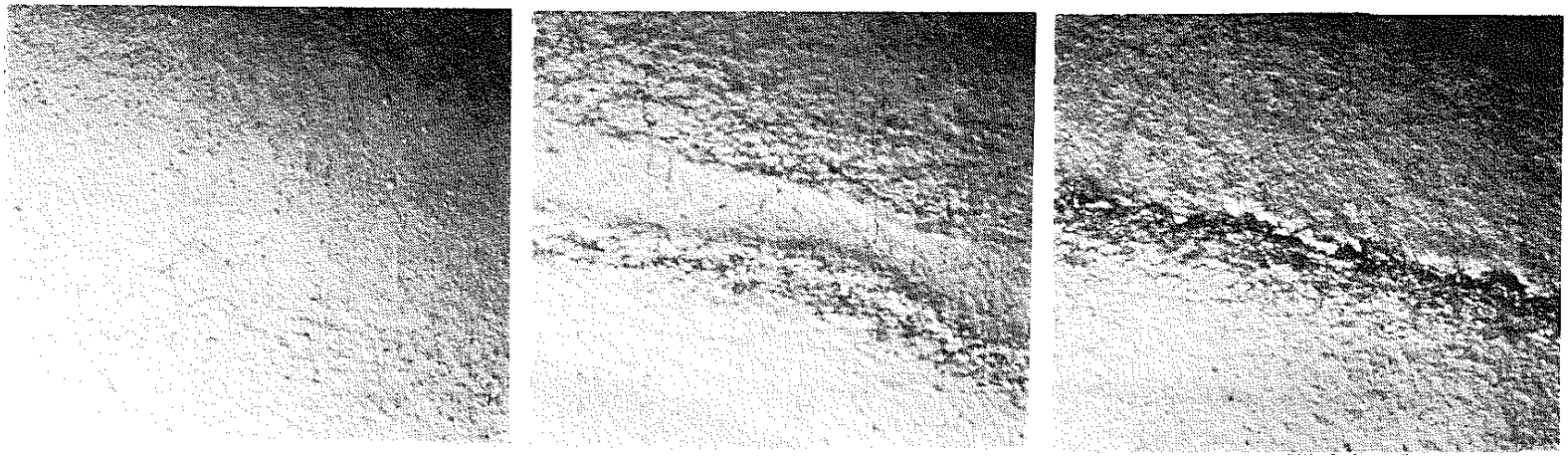

N = 1132 N = 1135 N = 1137

SAE 1045, (4527) TENSION, $\frac{\Delta\epsilon}{2} = 1\%$, $N_f = 1137$

1 mm

SPECIMEN AXIS

TYPE R CRACK SYSTEM - FAILURE OCCURS BY LINKING OF MICROCRACKS LATE IN LIFE.

Figure 14

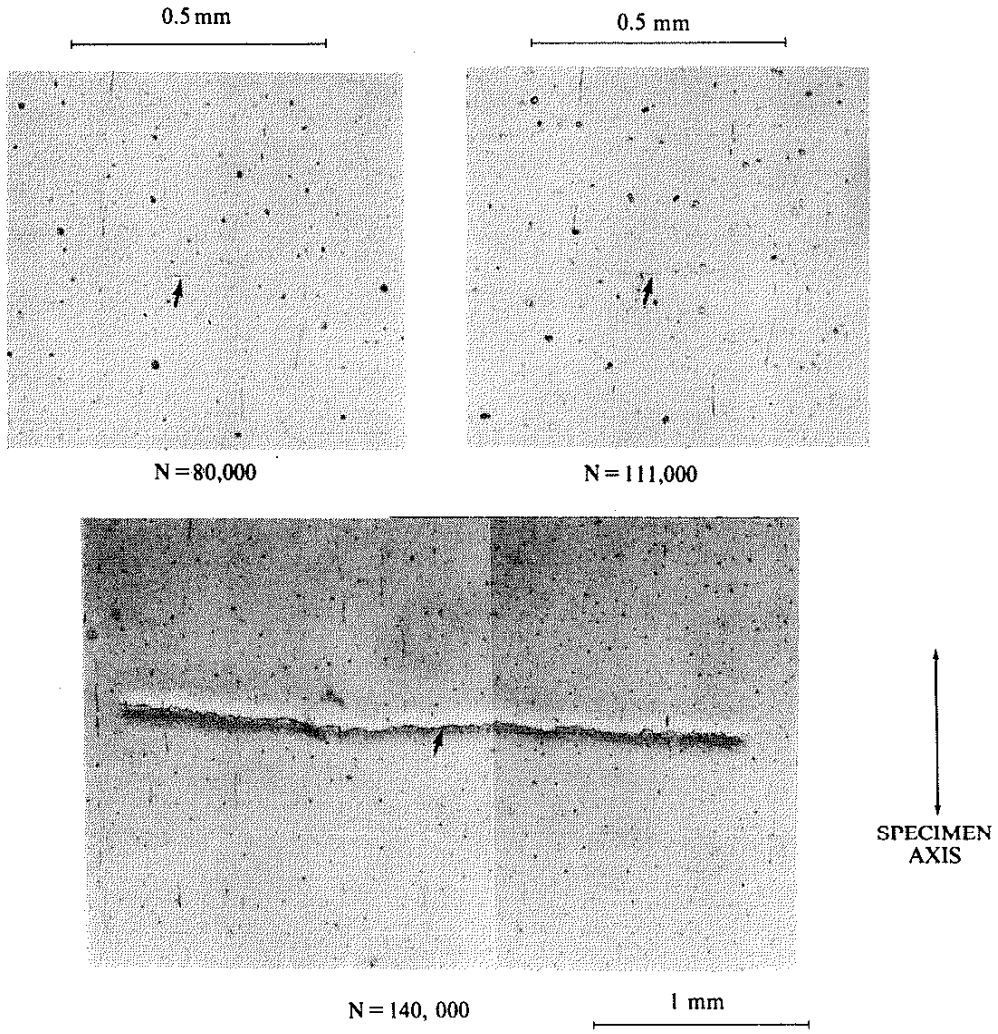

SAE 1045 (4511), TENSION, $\frac{\Delta\epsilon}{2} = 0.22\%$ $N_f = 142{,}500$

TYPE S CRACK SYSTEM - ONE DOMINANT CRACK GROWS UNTIL FAILURE

Figure 15

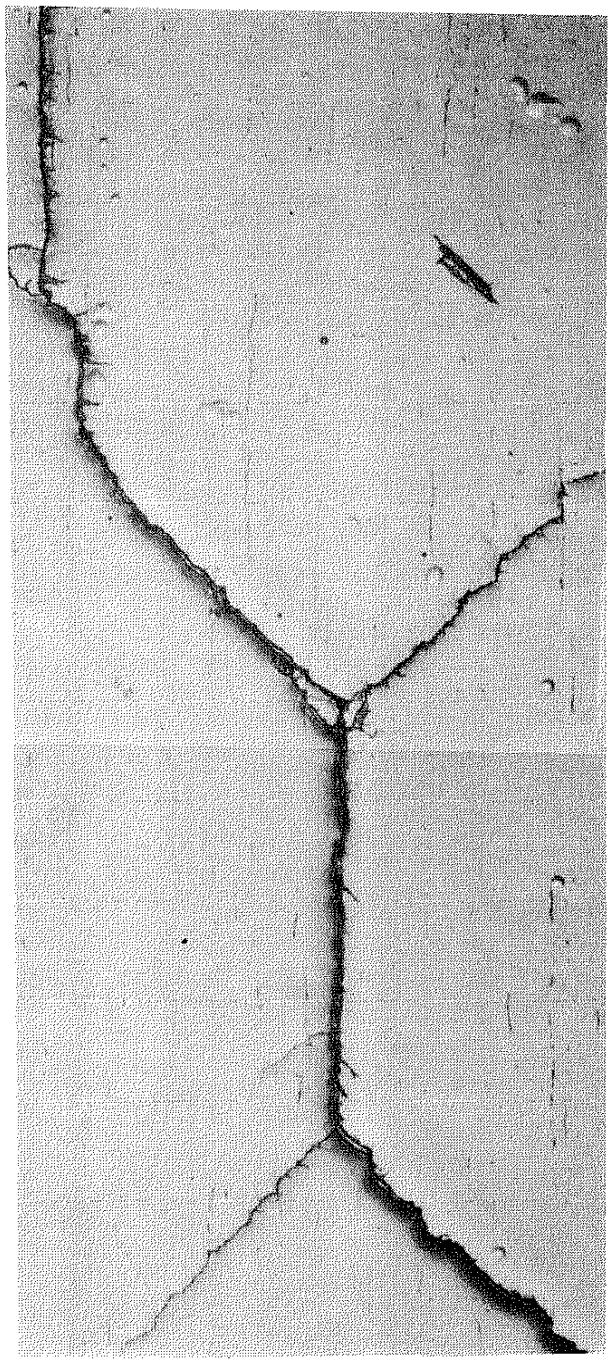

IN SAE 1045 REGION II BEHAVIOR OBSERVED AT LONG LIVES.

Figure 16

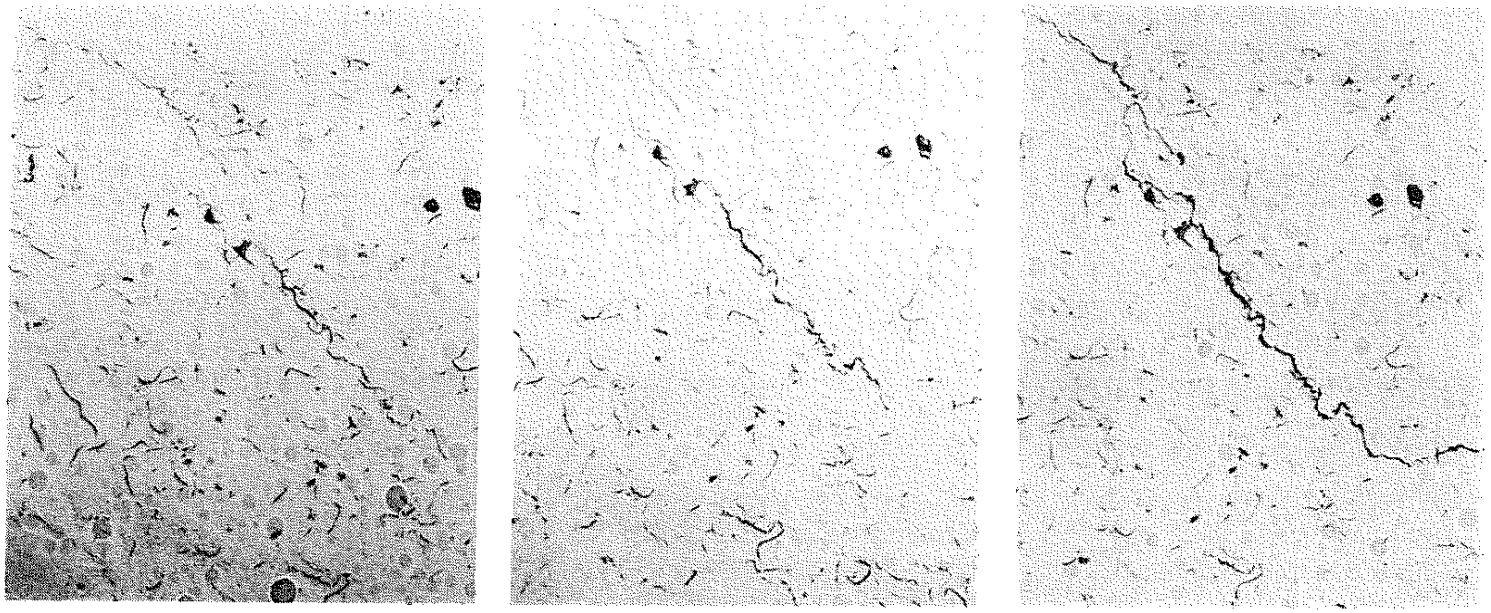

GRAY CAST IRON (NC01); $\frac{\Delta\gamma}{2} = 0.6\%$, $N_f = 440$

IN GRAY CAST IRON, CRACK GROWTH OCCURS BY LINKING OF GRAPHITE FLAKES ON TENSILE PLANES

Figure 17

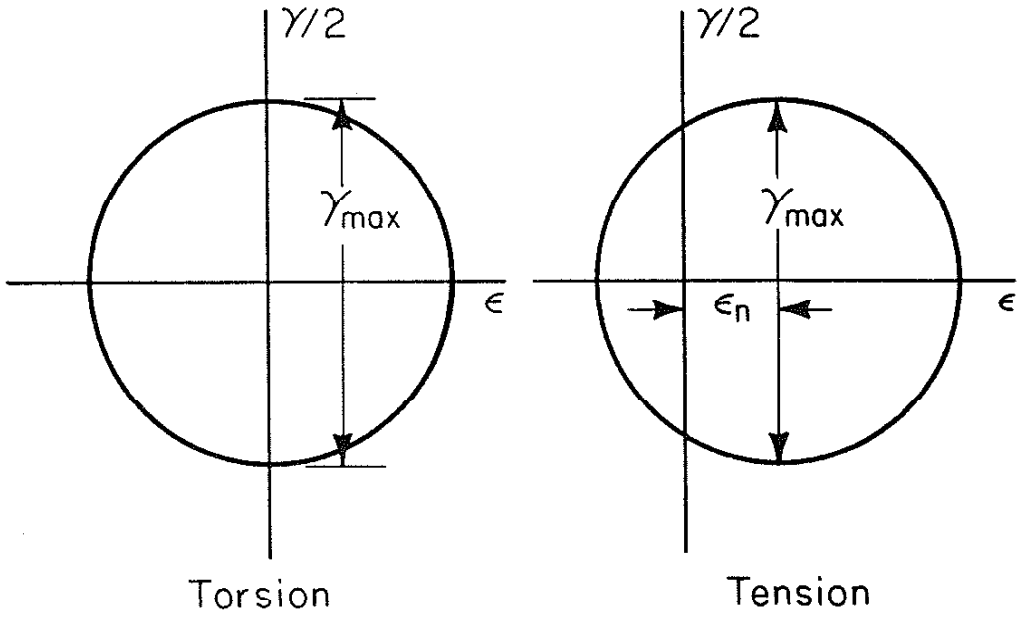

Torsion and Tension Strain States

Figure 18

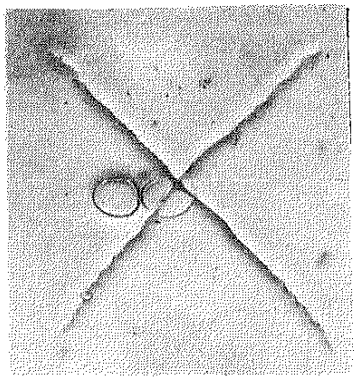

STAINLESS STEEL AISI 304 (SS09)

$\frac{\Delta\gamma}{2}$ = 0.35%

N = 1.0×10^6

N_f = 1.1×10^6

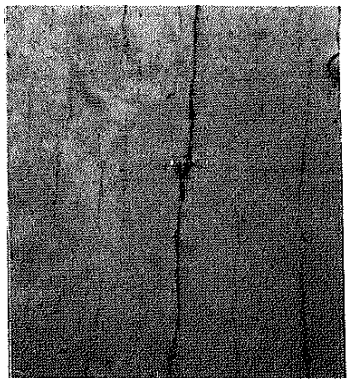

INCONEL 718 (IN13)

$\frac{\Delta\gamma}{2}$ = 1.7%

N = 1500

N_f = 1670

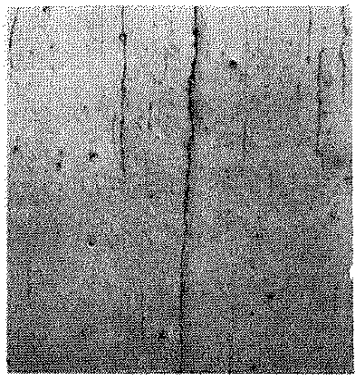

SAE 1045 (4531)

$\frac{\Delta\gamma}{2}$ = 0.38%

N = 90,000

N_f = 93052

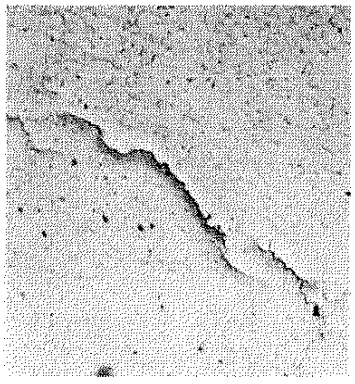

GRAY CAST IRON(NC01)

$\frac{\Delta\gamma}{2}$ = .006

N = 400

N_f = 440

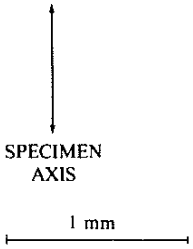

CRACKING BEHAVIOR OF FOUR MATERIALS AT RATIO OF PLASTIC/TOTAL STRAIN EQUAL TO 50%

Figure 19

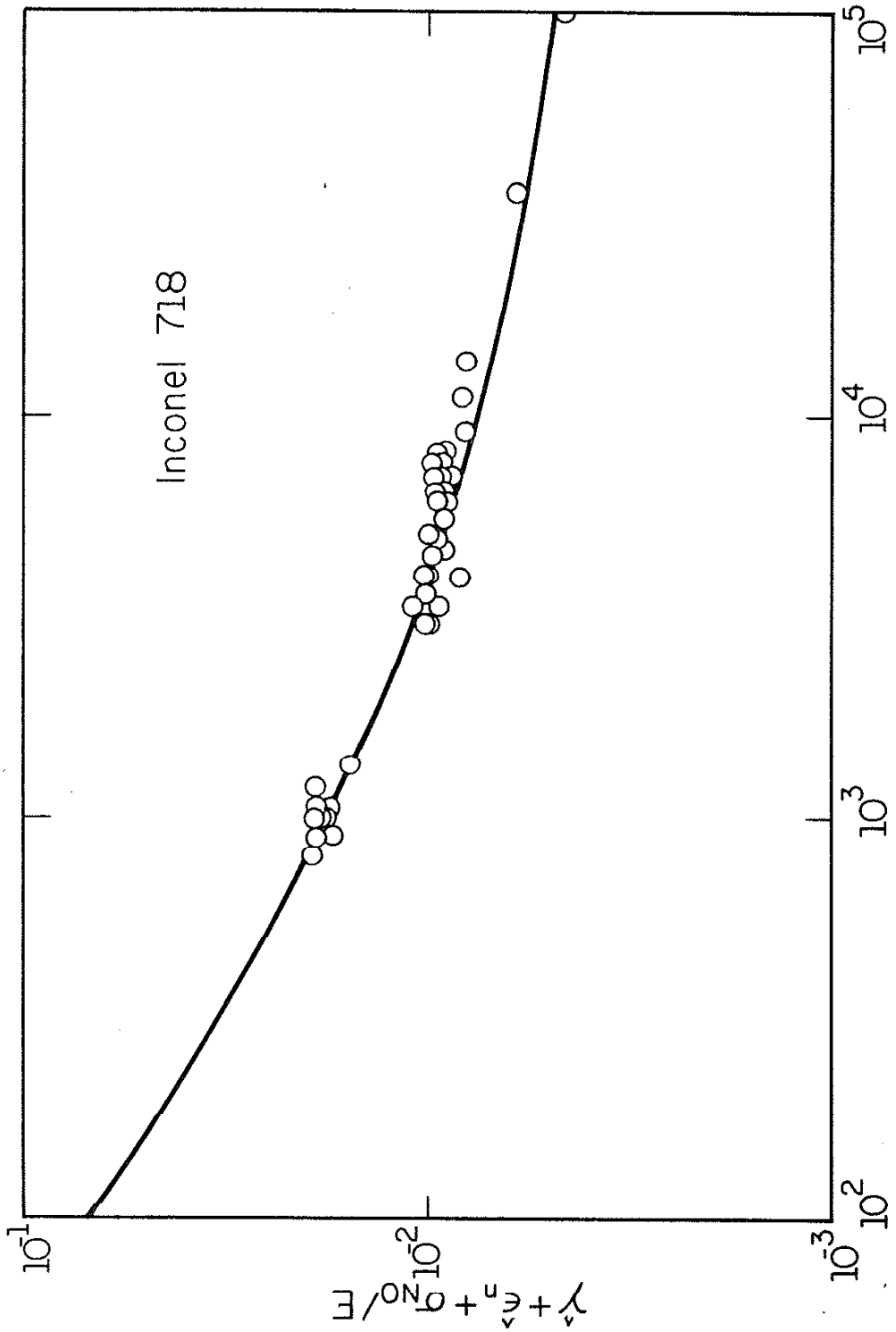

Correlation of Inconel 718 Test Results with Shear Strain Parameter

Figure 20

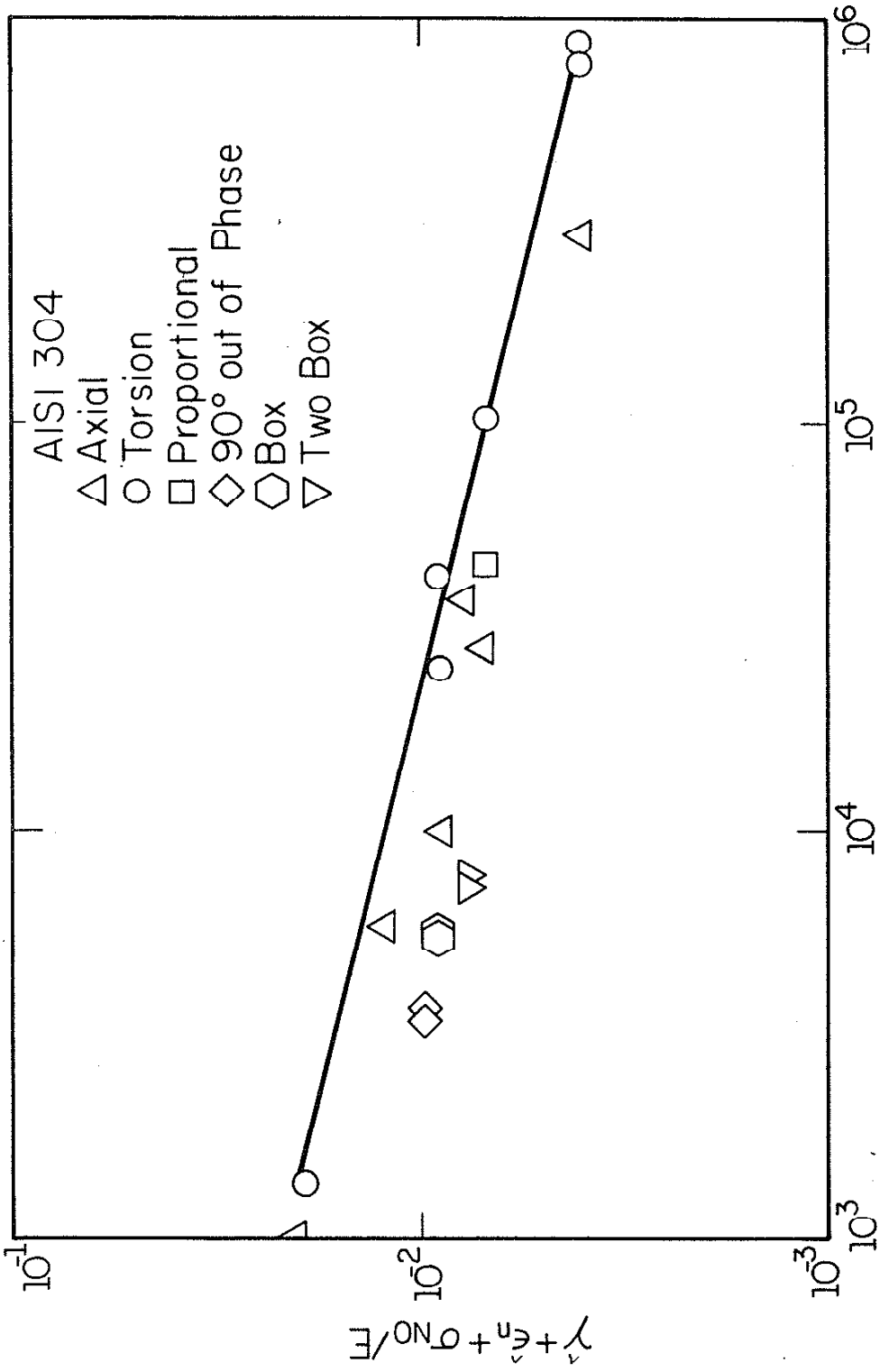

Correlation of AISI 304 Test Results with Shear Strain Parameter

Figure 21

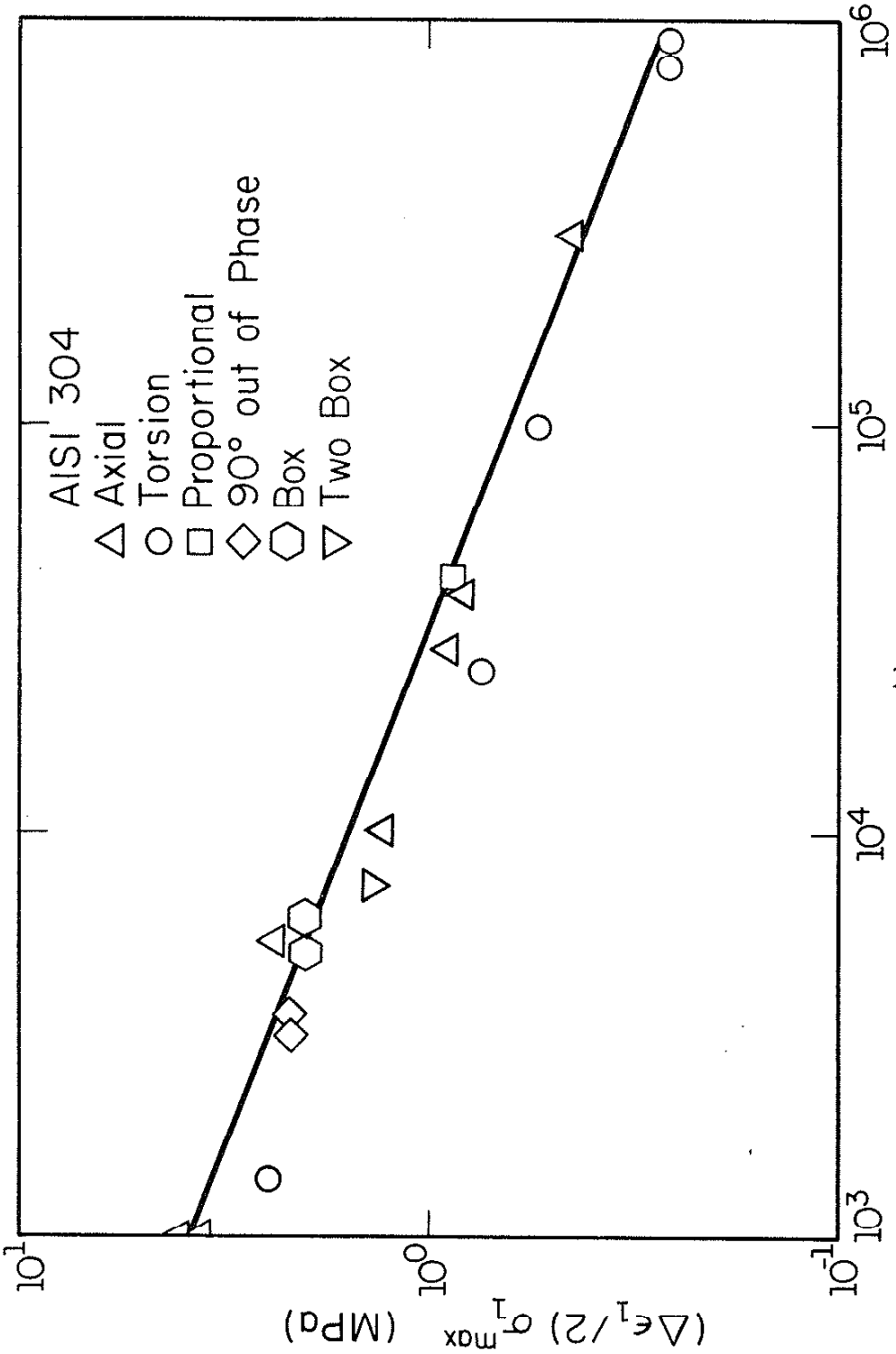

Correlation of AISI 304 Test Results with Maximum Principal Stress Parameter

Figure 22

APPENDIX A:

SMITH WATSON TOPPER PARAMETER IN MULTIAXIAL FATIGUE

LIST OF FIGURES

APPENDIX A

In this analysis, the Smith Watson Topper (SWT) parameter

$$\frac{\Delta\varepsilon}{2}\,\sigma_1^{max}$$

is interpreted such that the critical damage plane of the specimen is the plane experiencing the largest alternation of principal strain, $\frac{\Delta\varepsilon}{2}1$. The stress, σ_1^{max}, is the maximum value of normal stress acting on this plane.

It is important to note that although, ε_1^{max}, the maximum value of principal strain on the critical plane and σ_1^{max}, the maximum normal stress on this plane, occur at the same point on the loading path in the case of proportional loading, this is not always the case for a non-proportional history. An example of this is illustrated in Fig. A1, which is the axial stress-strain response on a horizontal plane for a 90 degree out-of-phase loading path. Although this is not the plane of maximum principal strain alternation for this load path, this hysteresis loop illustrates the fact that the maximum stress and maximum strain on a given plane do not necessarily occur at the same location in the loading path.

To determine the plane of maximum principal strain alternation, strain states are analyzed at discrete points in the path, analogous to the method described by Koch in Ref. [31]. Figure A.2 presents a non-proportional loading history and Mohr's circle representation of strain for 8 points during a cycle of loading. The "box path" represents one cycle. Point y in each of the figures represents the strain state on

the horizontal plane. As seen, the principal strain plane rotates continuously throughout the cycle. At Point A, the strain state is identical to that for a uniaxial load. At Point B, a combination of axial and torsional strains are applied. Consequently, the maximum principal strain for this loading condition is larger than that at Point A. Inspection of the strain-states of the loading path shows that this is the maximum principal strain for the total path. This principal strain occurs on a plane which is rotated counterclockwise by an angle α from the y-plane as shown in Fig. A.2ii. (The y-plane is the horizontal plane or a plane perpendicular to the specimen axis). The same value of principal strain also occurs at Point H (Fig. A.2viii) on a plane rotated clockwise by an angle α from the y-plane.

Considering the α plane associated with loading point B, the minimum value of principal strain on this plane occurs at Point F, which is also the point of minimum principal strain for the total loading path. An identical strain is again achieved at Point D and occurs on the α plane associated with Point H. Thus, for the box loading path shown, there are two planes of maximum principal strain alternation (This is due to the symmetry of the loading path.) The first plane associated with Points B and F, is oriented at an angle α counter-clockwise from the y plane, while the second, associated with Points D and H, is at an angle α clockwise from the y plane.

Plotted results of an analysis of the above loading case are shown in Figs. A.3 through A.5. Figure A.3a shows the input parameters or loading path for a strain-controlled "box path" test. Figure A3.b presents the corresponding axial and shear stress response acting on the

horizontal or y plane. Figures A.4a and A.4b show the axial and torsional stress-strain response on this same plane. As presented in Fig. A.2, the plane of maximum principal strain rotates with respect to the horizontal plane. The critical damage plane is the α plane rotated clockwise from the y plane. This corresponds to points D and H in Fig. A.2. As seen in Fig. A.3b, the normal stress at point H is greater than that at point B. Thus, due to the larger value of σ_1^{max}, the maximum value of the SWT parameter occurs on the α plane rotated clockwise from the horizontal. Figure A5 presents the stress-strain response on this critical plane.

Although the maximum stress, σ_1^{max}, and maximum strain, ϵ_1^{max} on the critical plane occur at the same point in the "box path" (Fig. A.5), this is not always the case for other non-proportional loading cases. As previously discussed (Fig. A.1), the maximum stress on the plane of maximum strain alternation, σ_1^{max}, does not always occur at the point of maximum strain for out of phase loading. Consequently, the stress on the critical plane must be continually monitored and the maximum value identified. The value of the SWT parameter is then simply the product of the principal strain alternation and the maximum stress on the critical plane.

Calculation methods and further discussion are found in Ref. [35].

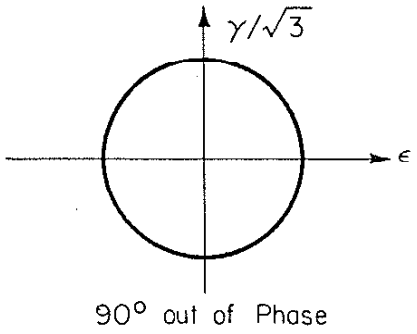

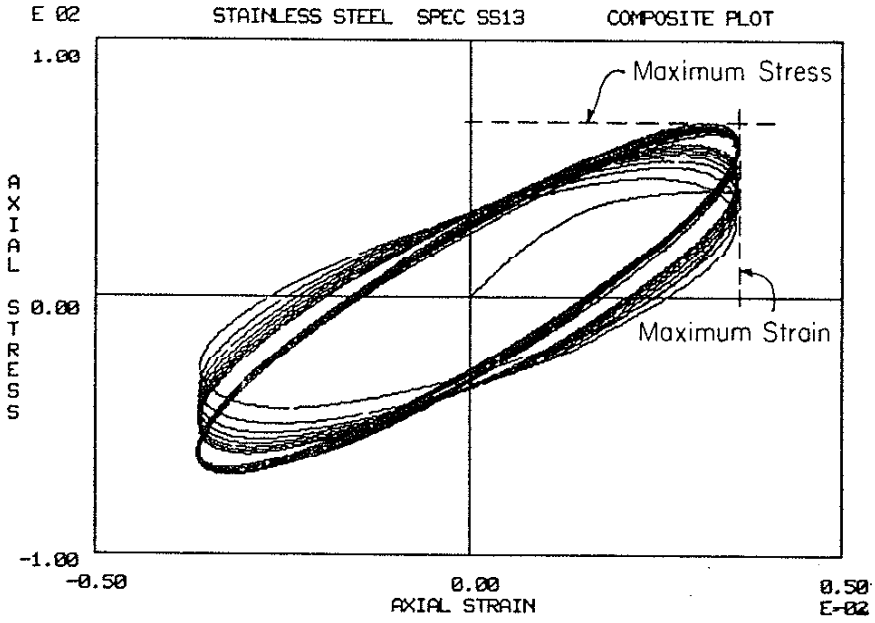

Figure A.1 Axial Stress-Strain Response on Horizontal Plane for 90° Out-of-Phase Loading

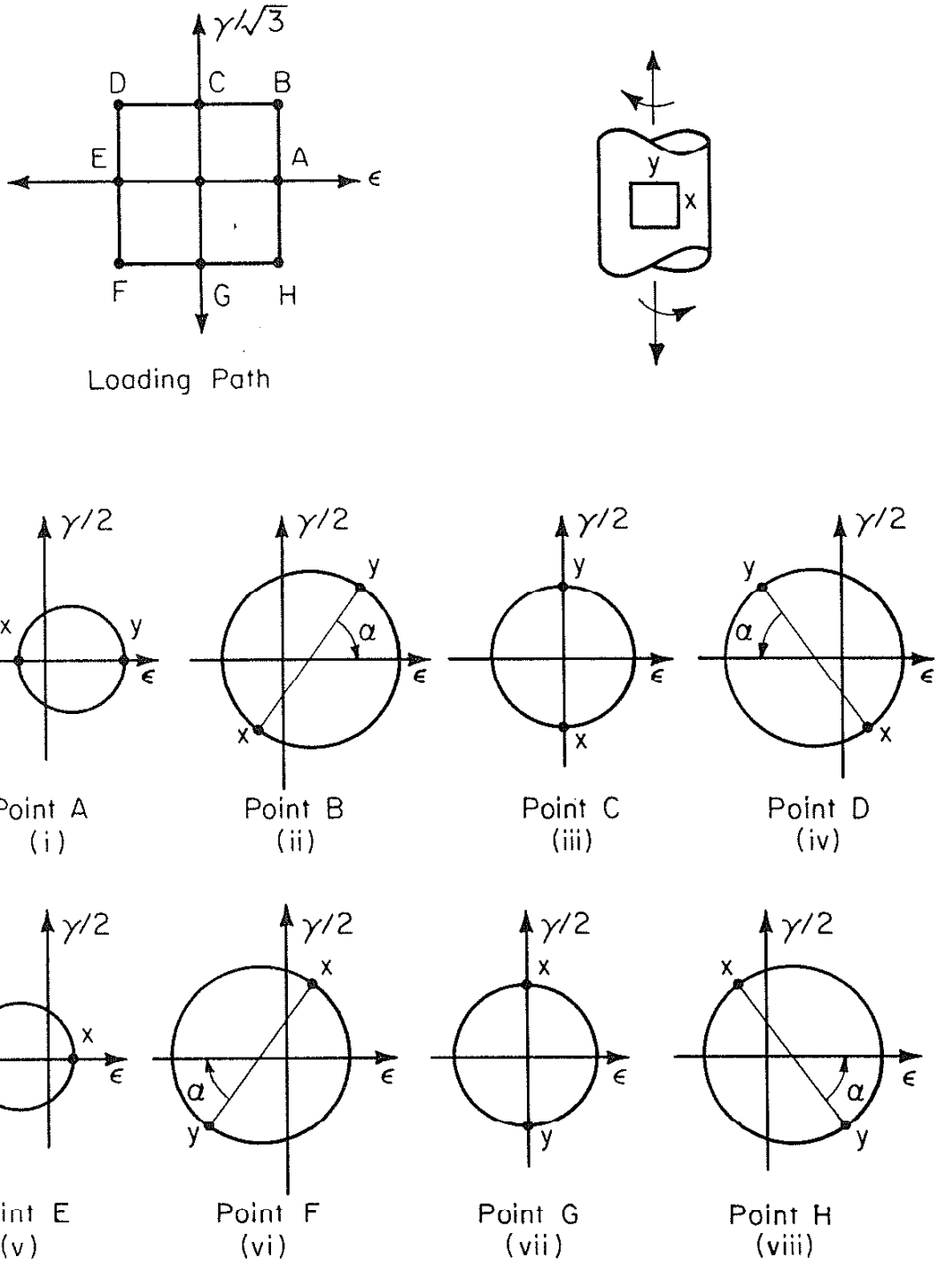

Figure A.2 Non-proportional "Box Path" Loading History and Mohr's Aid Representation of Strain for 8 Points in Cycle

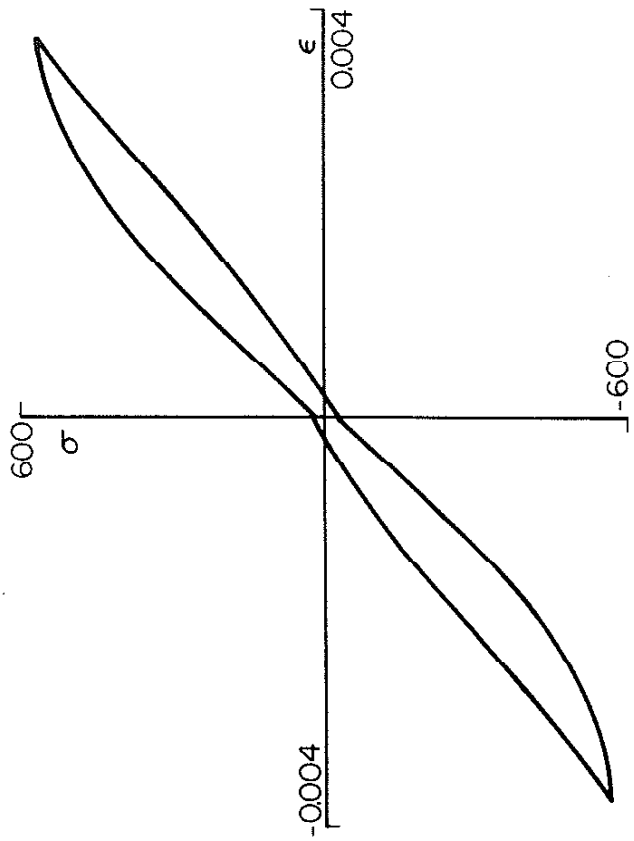

Figure A.5 Stress-Strain Response on the Plane of Maximum Principal Strain Alternation

APPENDIX B: SURFACE CRACK OBSERVATIONS

Page

LIST OF FIGURES

Stainless Steel 304

Stainless Steel 316

TORSION

$(R_\gamma = -1)$

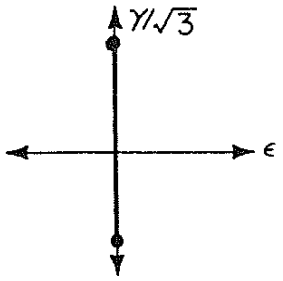

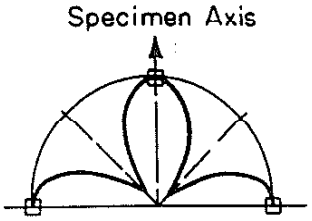

Polar Plot
Shear Strain Amplitude ($\hat{\gamma}$)
vs
Plane Angle (θ)

$$\begin{bmatrix} \frac{\Delta\gamma}{2} = 0.017 \\ \frac{\Delta\epsilon}{2} = 0 \end{bmatrix}$$

N=800
N_f=4090
SS-08

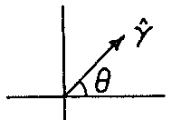

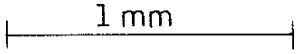

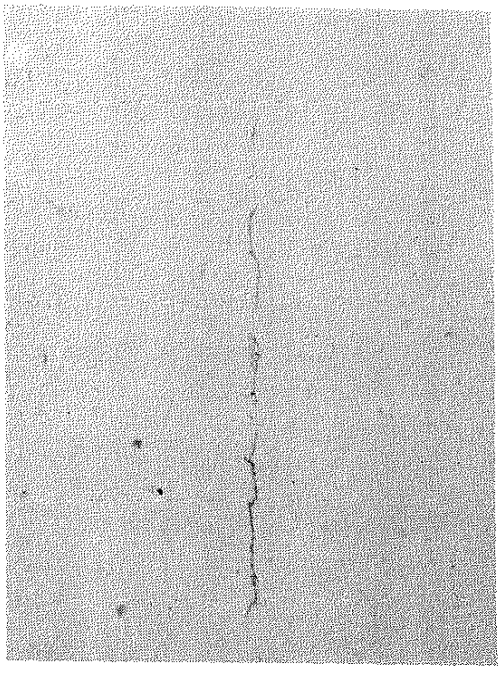

Specimen Axis

Figure B.1 SS08, $\frac{\Delta\gamma}{2} = 0.0173$

TORSION
(R_γ=-1)

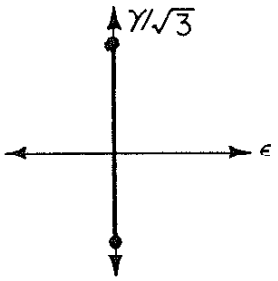

$$\left[\begin{array}{l} \frac{\Delta\gamma}{2}=0.008 \\ \frac{\Delta\epsilon}{2}=0 \end{array}\right]$$

N=48,000
N_f=48,500
SS-05

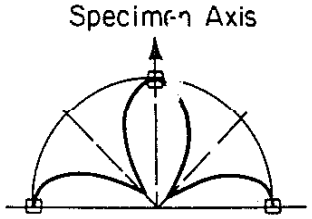

Polar Plot
Shear Strain Amplitude ($\hat{\gamma}$)
vs
Plane Angle (θ)

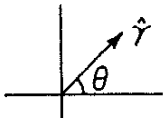

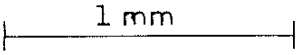

Specimen Axis

Figure B.2 SS05, $\frac{\Delta\gamma}{2}$ = 0.008

TORSION

$(R_\gamma = -1)$

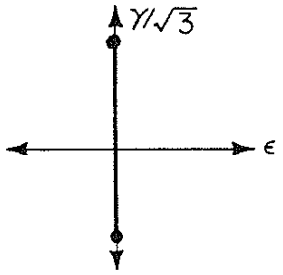

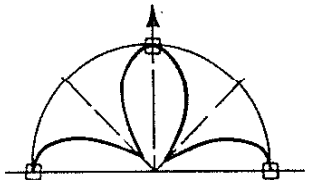

Polar Plot
Shear Strain Amplitude ($\hat{\gamma}$)
vs
Plane Angle (θ)

$$\left[\begin{array}{l} \frac{\Delta\gamma}{2} = 0.008 \\ \frac{\Delta\epsilon}{2} = 0 \end{array}\right]$$

N = 30,000
N_f = 32,100
SS21

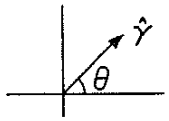

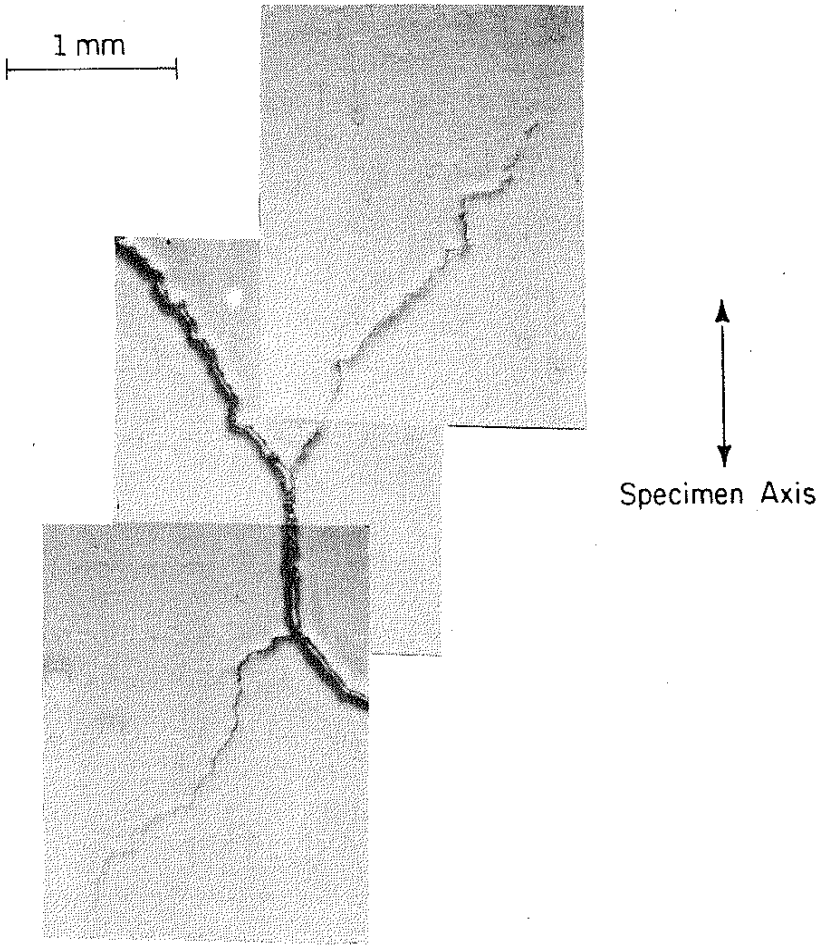

Figure B.3 SS21, $\frac{\Delta\gamma}{2} = 0.008$

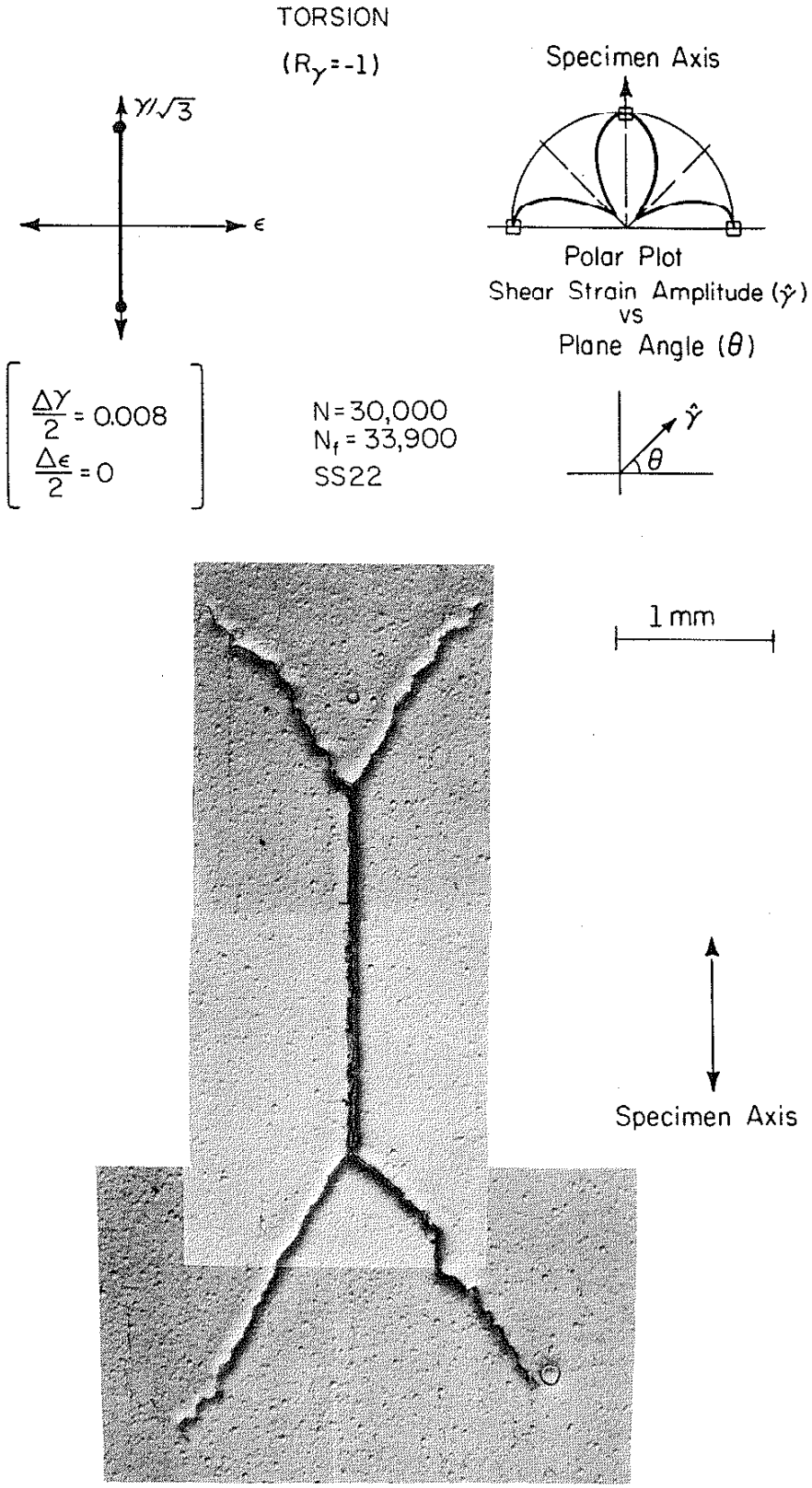

Figure B.4 SS22, $\frac{\Delta\gamma}{2} = 0.008$

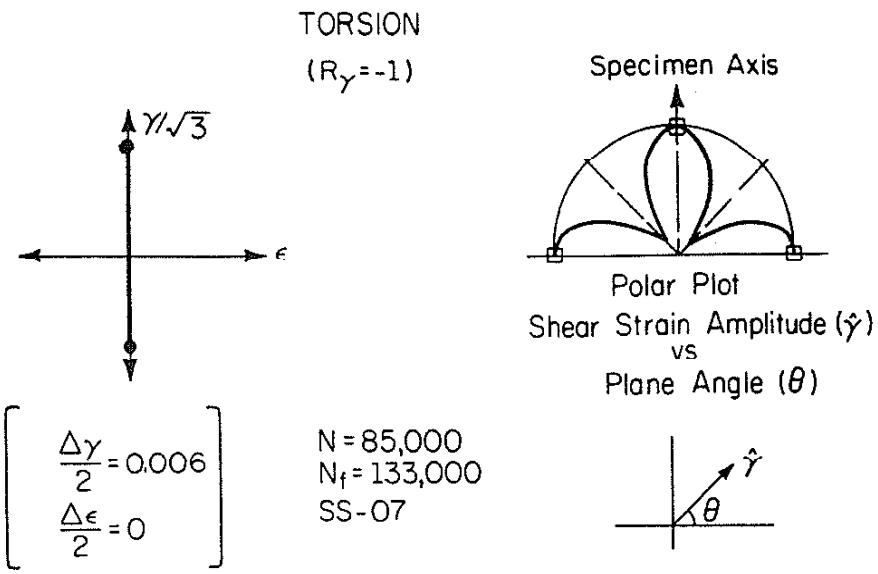

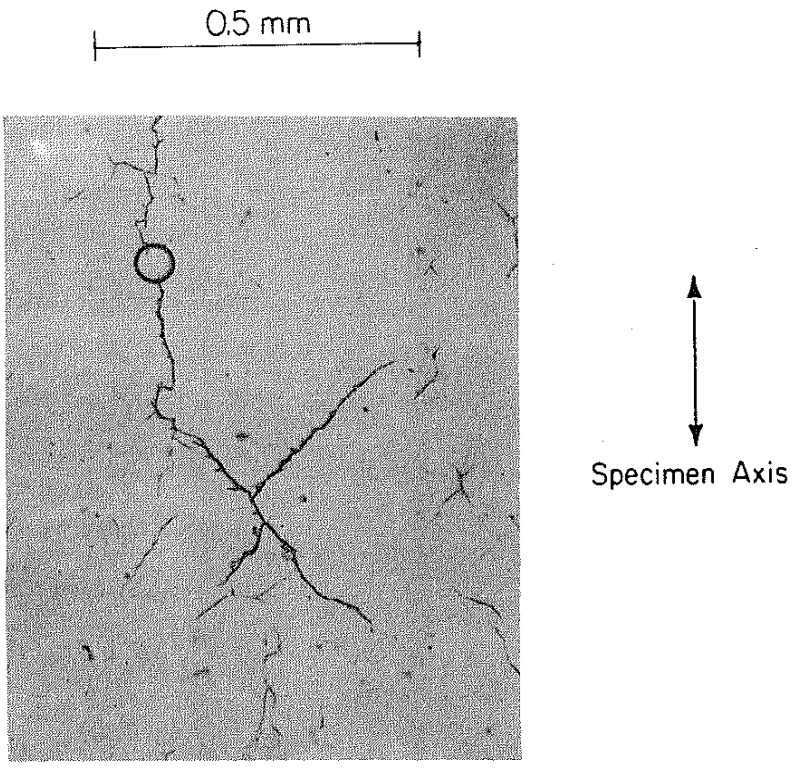

Figure B.5 SS07, $\frac{\Delta\gamma}{2} = 0.006$

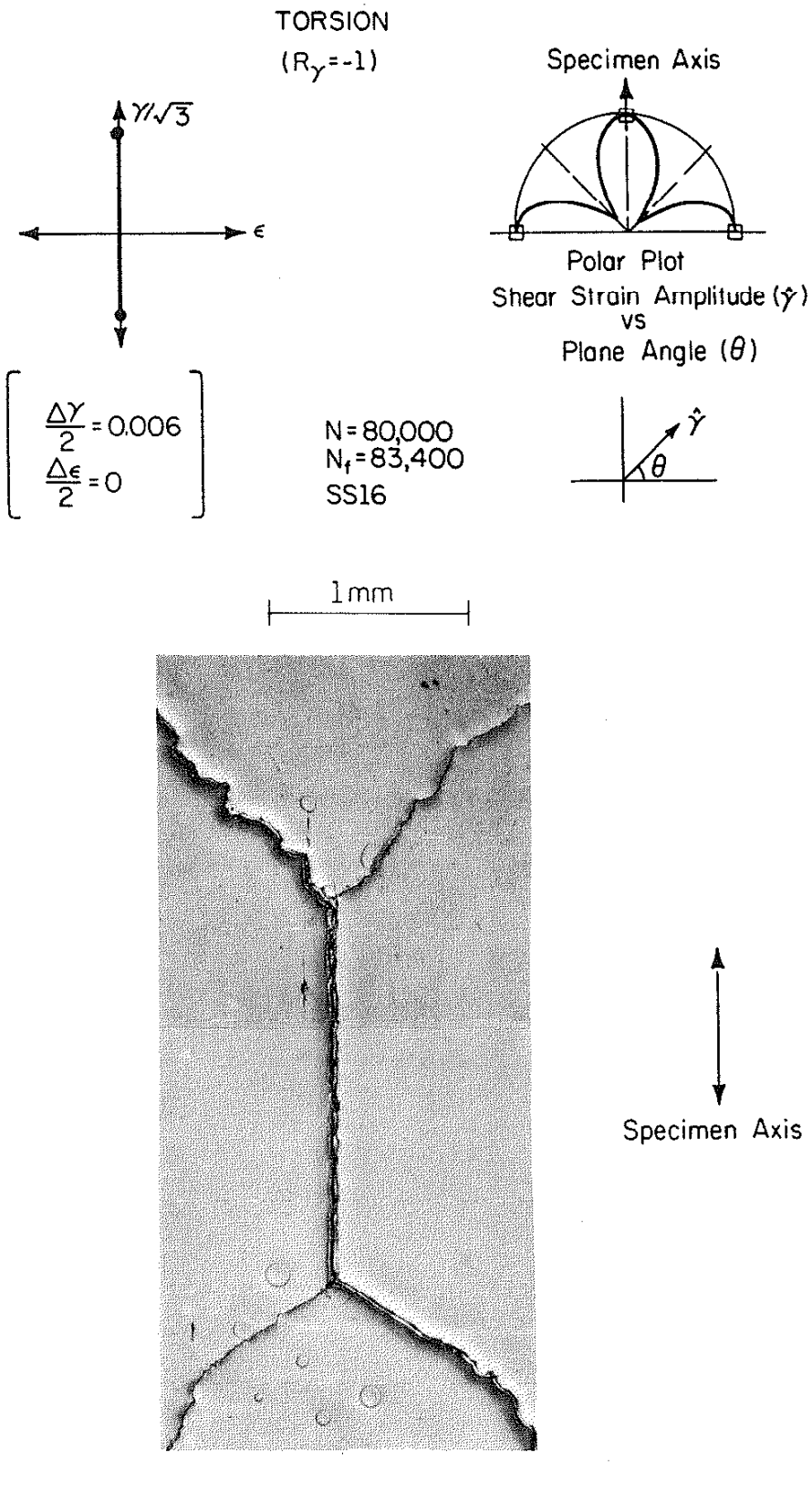

Figure B.6 SS16, $\frac{\Delta\gamma}{2} = 0.006$

TORSION

($R_\gamma = -1$)

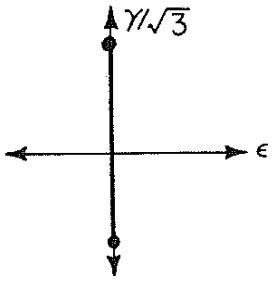

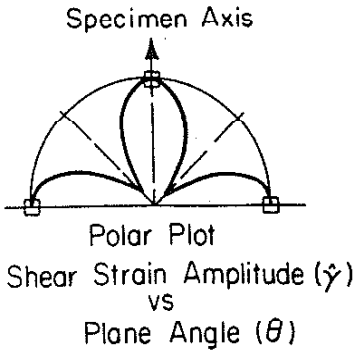

$$\left[\begin{array}{l} \frac{\Delta\gamma}{2} = 0.0035 \\ \frac{\Delta\epsilon}{2} = 0 \end{array}\right]$$

N = 700,000
$N_f = 1.1 \times 10^6$
SS-09

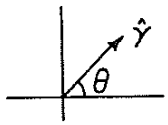

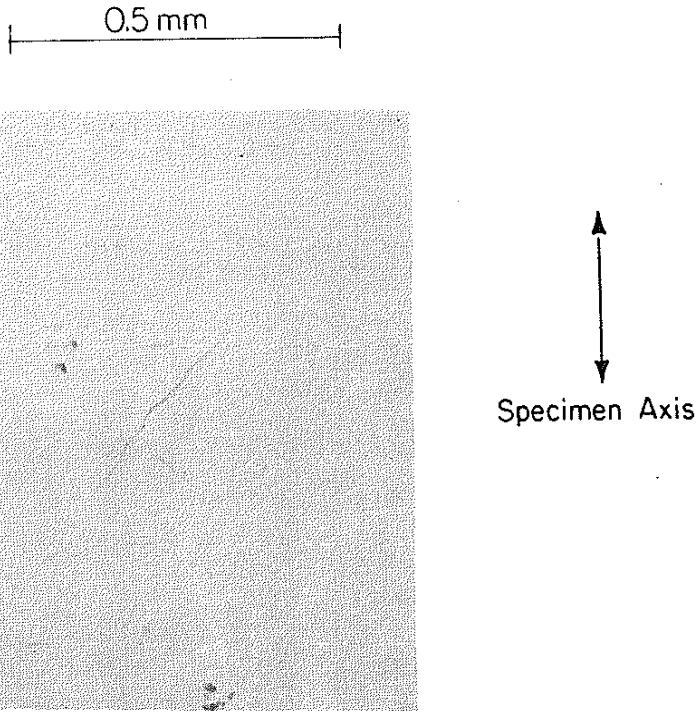

Figure B.7 SS09, $\frac{\Delta\gamma}{2} = 0.0035$

TORSION

$(R_\gamma = -1)$

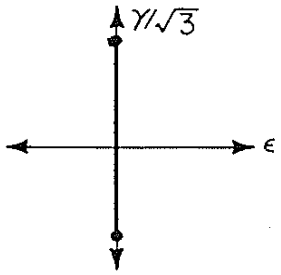

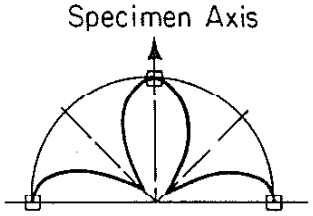

Polar Plot
Shear Strain Amplitude ($\hat{\gamma}$)
vs
Plane Angle (θ)

$\frac{\Delta\gamma}{2} = 0.0035$

$\frac{\Delta\epsilon}{2} = 0$

N = 750,000
N_f = 824,200
SS20

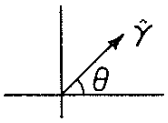

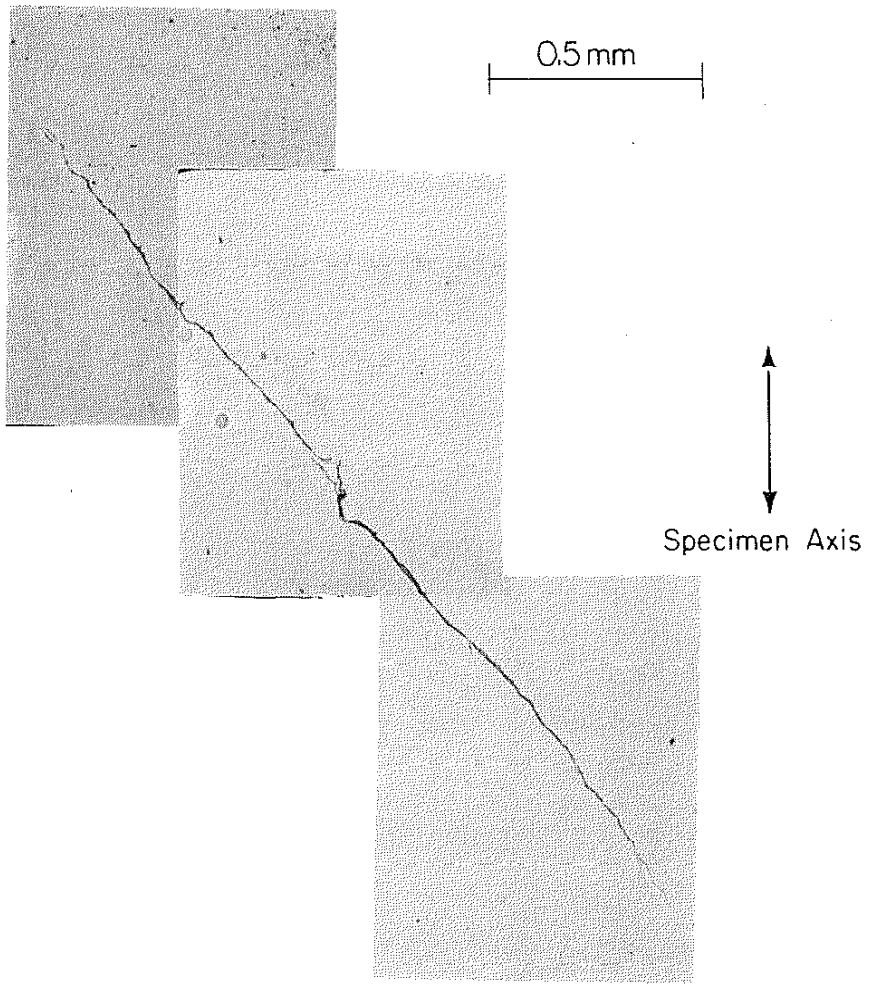

Figure B.8 SS20, $\frac{\Delta\gamma}{2} = 0.0035$

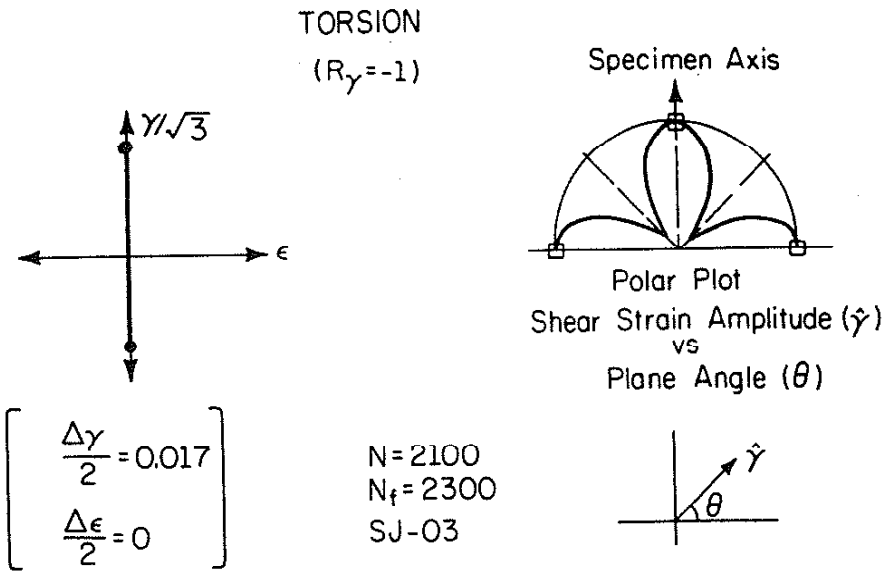

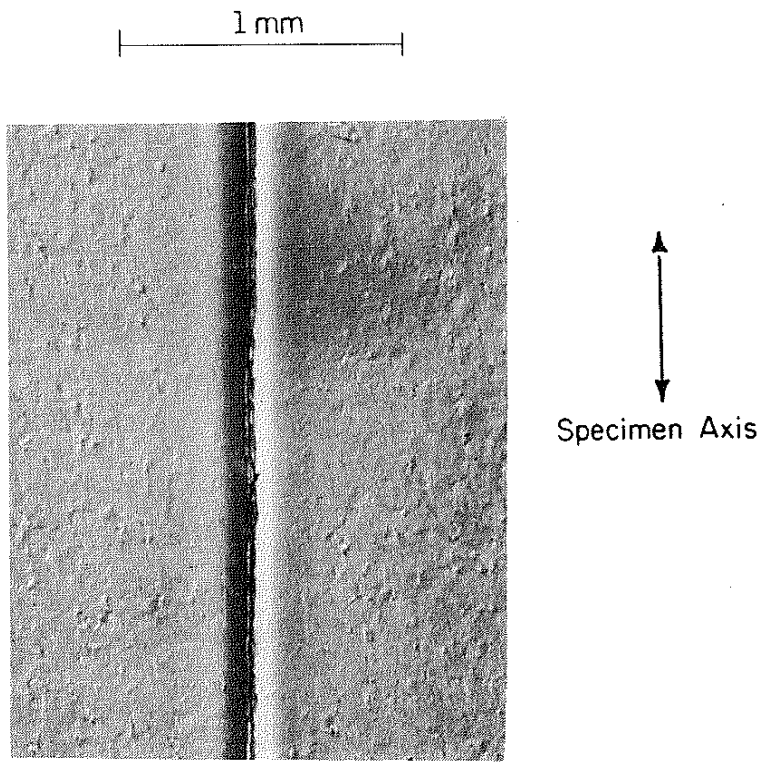

Figure B.9 SJ03, $\frac{\Delta\gamma}{2} = 0.0173$

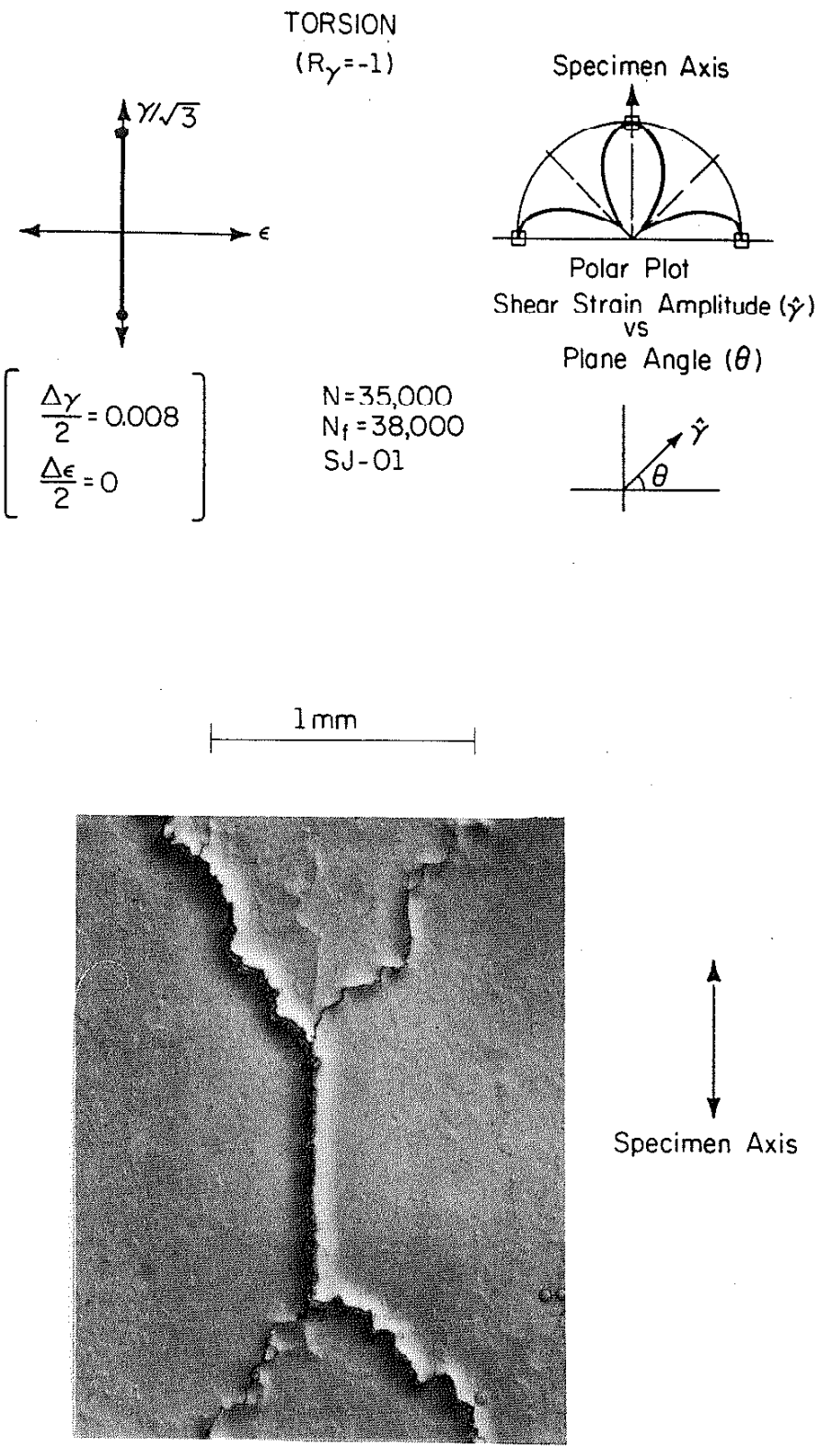

Figure B.10 SJ01, $\frac{\Delta\gamma}{2}$ = 0.008

TORSION

$(R_\gamma = -1)$

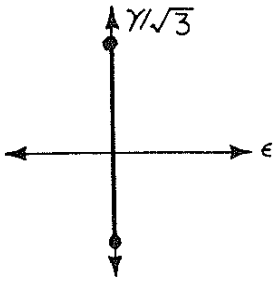

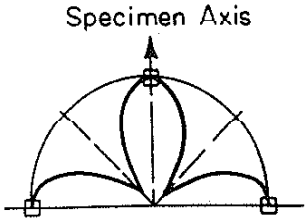

Polar Plot
Shear Strain Amplitude ($\hat{\gamma}$)
vs
Plane Angle (θ)

$$\begin{bmatrix} \frac{\Delta\gamma}{2} = 0.006 \\ \frac{\Delta\epsilon}{2} = 0 \end{bmatrix}$$

N = 90,000
N_f = 100,000
SJ-02

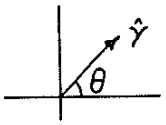

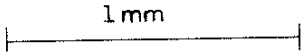

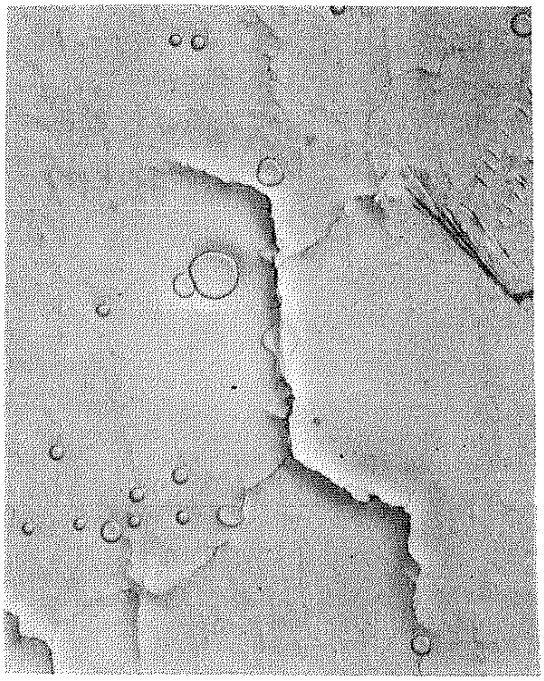

Specimen Axis

Figure B.11 SJ02, $\frac{\Delta\gamma}{2}$ = 0.006

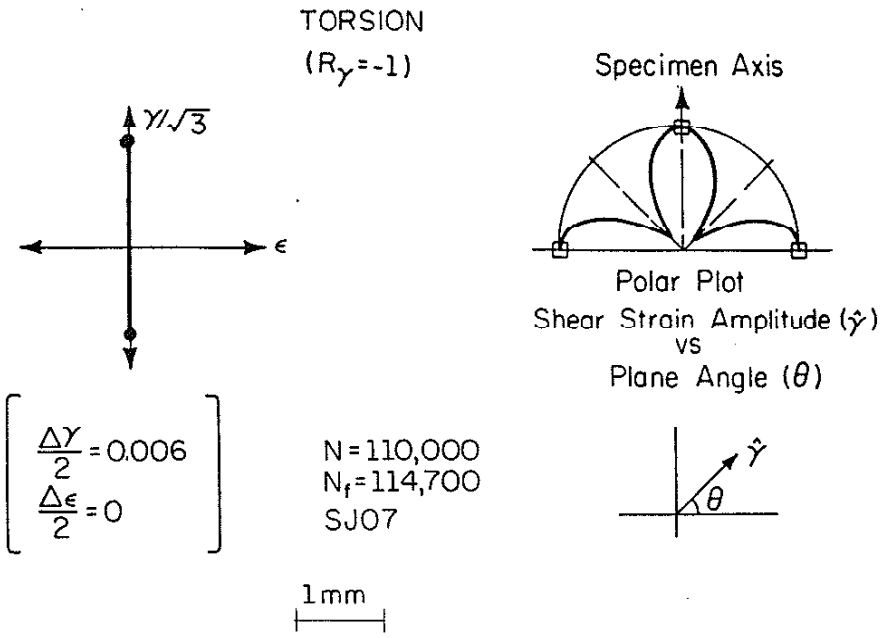

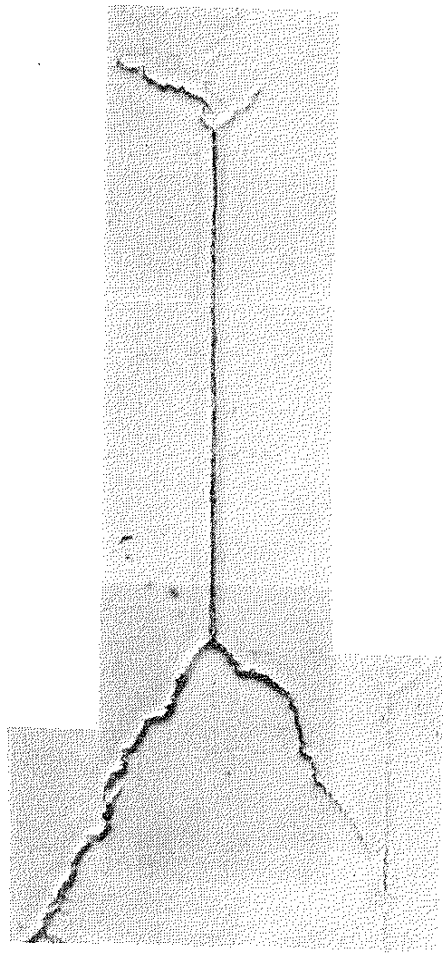

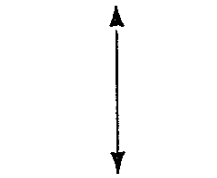

Figure B.12 SJ07, $\frac{\Delta\gamma}{2} = 0.006$

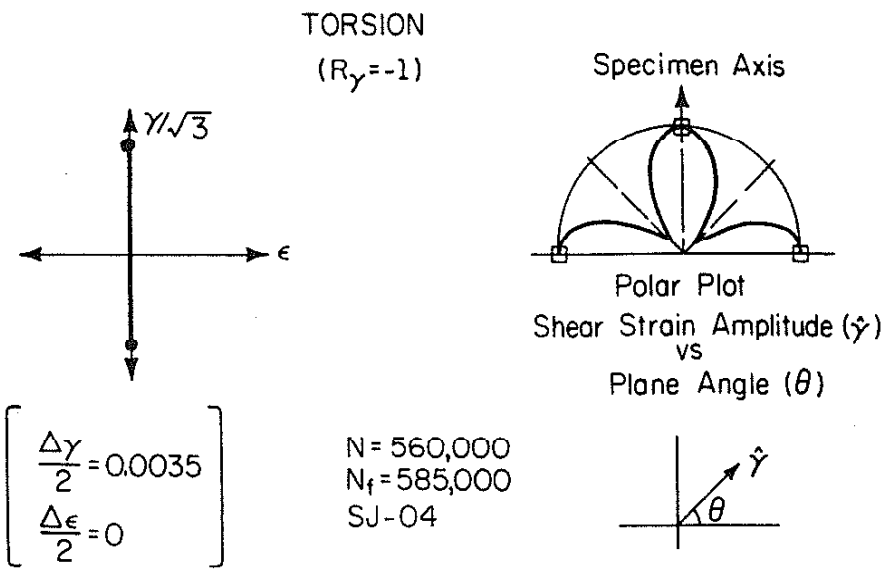

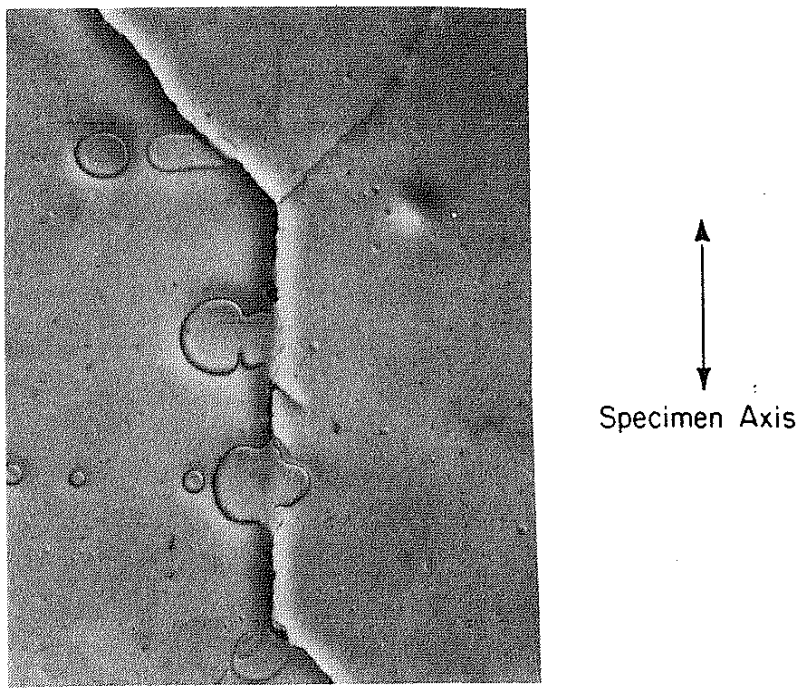

Figure B.13 SJ04, $\frac{\Delta\gamma}{2}$ = 0.0035

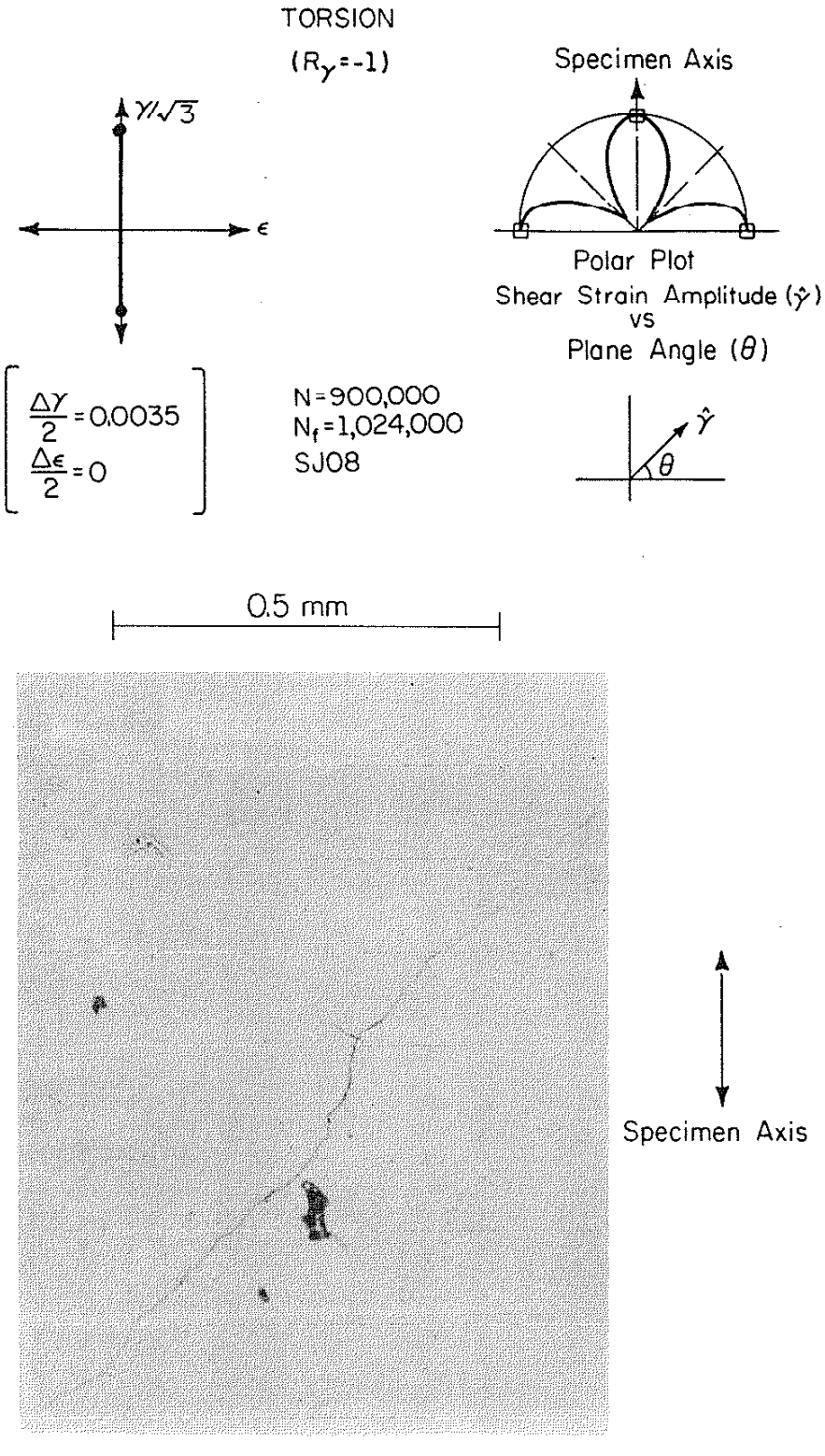

Figure B.14 SJ08, $\frac{\Delta\gamma}{2} = 0.0035$

TORSION

$(R_\gamma = -1)$

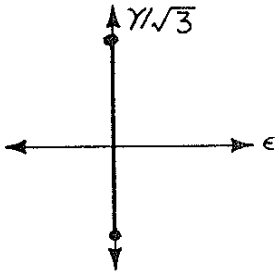

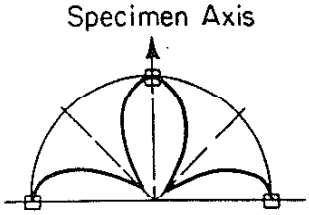

Polar Plot
Shear Strain Amplitude ($\hat{\gamma}$)
vs
Plane Angle (θ)

$$\begin{bmatrix} \frac{\Delta\gamma}{2} = 0.003 \\ \frac{\Delta\epsilon}{2} = 0 \end{bmatrix}$$

N = 900,000
N_f = 939,500
SJ06

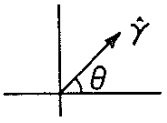

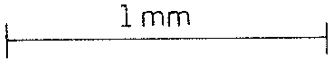

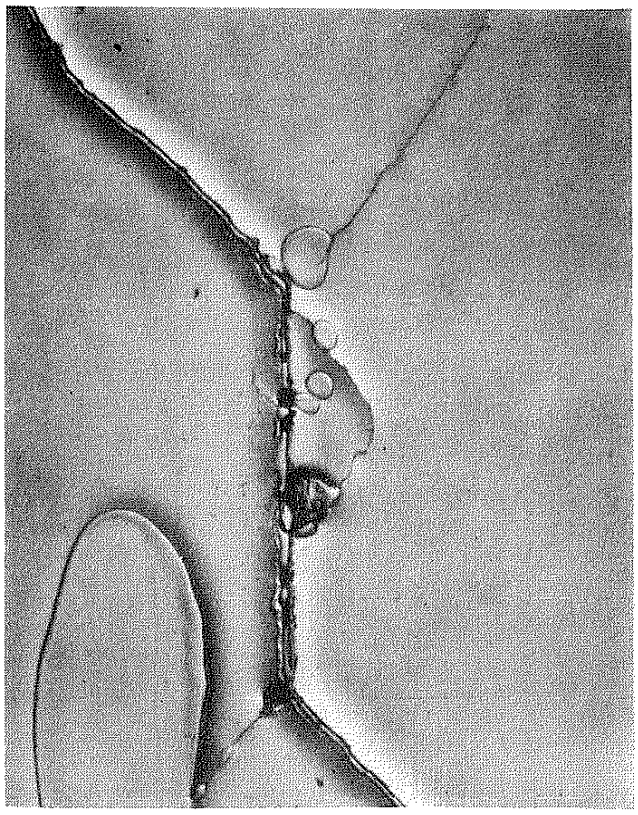

Specimen Axis

Figure B.15 SJ06, $\frac{\Delta\gamma}{2} = 0.0030$

APPENDIX C: CRACK GROWTH DATA

Page

LIST OF TABLES

Stainless Steel 304

Stainless Steel 316

APPENDIX C

Acetate replicas were taken of the specimen surface features at intervals of approximately 10 percent of predicted fatigue life. Crack measurements were made from microscopic inspection of these replicas.

In general, four crack measurements were made from each replica of the AISI 304 and 316 specimens tested in torsion. These are represented graphically in Fig. C.1. Four branch cracks or legs usually grew from the main shear crack, a_2, as seen in Fig. C.1a. These branch or tensile (Stage II) cracks were oriented approximately 45 degrees to the axis of the specimen. Cracks a_1 and a_3 represent the lengths of the dominant branch cracks. These were usually the longest tensile cracks and the first to branch off the main shear crack. The total crack length, L, was measured "as the crow flies" as shown in Fig. C.1b.

No crack measurements were obtained for AISI 304 and 316 specimens tested in tension as the crack initiated from the inside surface of the specimen. Cracks were observed on outside surface replicas only very late in life when the crack had grown through the wall thickness.

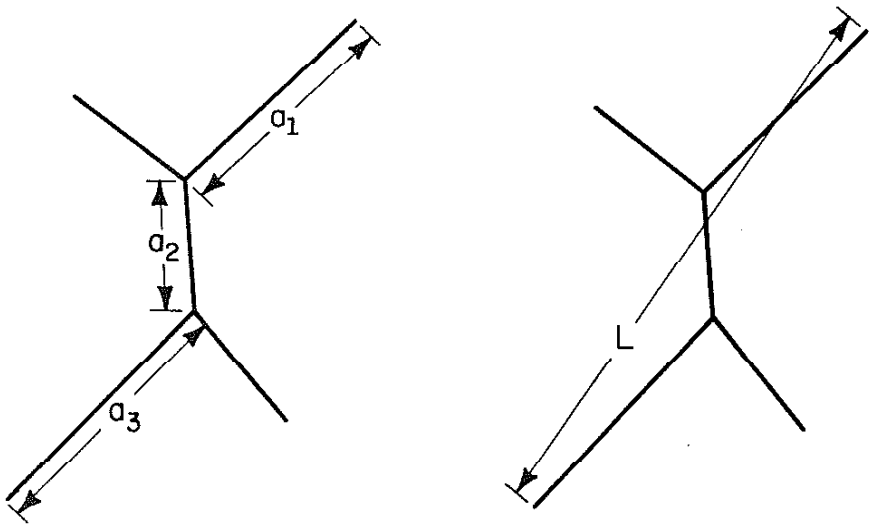

Figure C.1 Crack Length Measurements

Table C.1
Stainless Steel 304
Crack Growth Data
Specimen I.D. SS08

$R_\varepsilon = 0$ $R_\gamma = -1$

$\frac{\Delta\varepsilon}{2} = 0$ $\frac{\Delta\gamma}{2} = 0.0173$

N (Cycles)	L (mm)	Comments
4,000	16.9	Crack grows generally in shear.
3,500	4.89	(No a_1 or a_3 cracks.) Some
3,000	3.23	branching from main crack occurs,
2,800	2.65	but main shear crack continues to
2,600	2.20	develop simultaneously.
2,400	1.94	
2,200	1.80	
2,000	1.74	
1,600	1.25	
1,400	1.03	
1,200	0.77	
1,000	0.55	
900	0.48	
800	0.47	
700	0.46	
600	0.45	
500	0.42	
400	0.40	
300	0.28	
200	0.28	
100	0.009	
50	0.008	
0	0	

Table C.2
Stainless Steel 304
Crack Growth Data
Specimen I.D. SS05

$R_\varepsilon = 0$ $R_\gamma = -1$

$\frac{\Delta\varepsilon}{2} = 0$ $\frac{\Delta\gamma}{2} = 0.008$

N (Cycles)	L (mm)	a_1 (mm)	a_2 (mm)	a_3 (mm)	Comments
48,000	3.16	1.42	0.07	1.67	
46,000	1.78	0.66	0.07	1.05	High crack density
45,000	1.68	0.64	0.07	0.94	
40,000	0.77	0.34	0.07	0.38	
35,000	0.43	0.17	0.07	0.21	
32,000	0.32	0.10	0.07	0.19	
30,000	0.28	----	0.07	----	Bubble on replica
28,000	0.24	0.07	0.07	0.11	
26,000	0.19	0.06	0.07	0.10	
24,000	0.17	0.05	0.07	0.09	
22,000	0.17	0.04	0.07	0.09	
20,000	0.15	0.03	0.07	0.08	
18,000	0.15	0.03	0.07	0.08	
13,000	0.09	~0.01	0.07	0.03	
9,000	0.08	0	0.07	0.01	
6,000	0.03	0	0.03	0	
4,000	~0	0	0	0	Crack visible but too fuzzy to measure length
3,500	0	0	0	0	No crack visible

Table C.3
Stainless Steel 304
Crack Growth Data
Specimen I.D. SS21

$R_\varepsilon = 0$ $R_\gamma = -1$

$\frac{\Delta\varepsilon}{2} = 0$ $\frac{\Delta\gamma}{2} = 0.008$

N (Cycles)	L (mm)	a_1 (mm)	a_2 (mm)	a_3 (mm)	Comments
32,000	> 10	8.4	1.0	8.34	Crack length a_2 is an estimate
30,000	5.58	2.70	0.95	1.48	
28,000	4.02	1.86	0.93	1.45	
26,000	2.89	1.14	0.92	0.92	
24,000	2.22	0.92	0.91	0.70	
22,000	2.02	0.66	0.90	0.51	
20,000	1.64	0.47	0.90	0.37	
18,000	1.47	0.36	0.89	0.28	
16,000	1.31	0.30	0.89	0.22	
14,000	1.20	0.20	0.89	0.18	
12,000	1.13	0.16	0.89	0.12	
10,000	1.08	0.15	0.89	0.09	
8,000	1.06	0.12	0.89	0.08	
6,000	0.97	0.06	0.89	0.04	
4,000	0.94	0.04	0.89	0.03	
2,000	0.89	0	0.89	0	Crack grows out of stringer or group of inclusions

Table C.4
Stainless Steel 304
Crack Growth Data
Specimen I.D. SS22

$R_\varepsilon = 0$ $\quad R_\gamma = -1$

$\frac{\Delta\varepsilon}{2} = 0$ $\quad \frac{\Delta\gamma}{2} = 0.008$

N Cycles	L (mm)	a_1 (mm)	a_2 (mm)	a_3 (mm)	Comments
32,000	8.01	3.34	2.25	2.71	
30,000	5.44	1.88	2.25	1.54	
27,500	4.01	1.11	2.25	0.89	
25,000	3.40	0.97	2.25	0.48	
22,500	3.03	0.61	2.25	0.42	
20,000	2.72	0.43	2.25	0.20	
17,500	~2.54	0.33	2.25	--	
15,000	2.44	0.23	2.25	0.10	
12,500	2.39	0.16	2.25	0.06	
10,000	2.34	0.11	2.25	0.03	a_3 branching occurs
7,500	2.34	0.08	2.25	0	
5,000	2.25	0.07	2.25	0	
2,500	2.25	0.04	2.25	0	
1,000	2.25	0.02	2.25	0	Immediate branching at inclusion

Table C.5
Stainless Steel 304
Crack Growth Data
Specimen I.D. SS07

$R_\varepsilon = 0$ $R_\gamma = -1$

$\frac{\Delta\varepsilon}{2} = 0$ $\frac{\Delta\gamma}{2} = 0.006$

N (Cycles)	L (mm)	a_1 (mm)	a_2 (mm)	a_3 (mm)	Comments
130,000	7.51	3.50	0.04	3.67	
125,000	3.71	1.63	0.04	2.05	
120,000	2.55	1.23	0.04	1.28	
115,000	2.29	0.98	0.04	0.96	
110,000	1.31	0.61	0.04	0.60	
105,000	1.20	0.37	0.04	0.60	
100,000	0.95	0.37	0.04	0.56	
95,000	0.48	0.21	0.04	0.40	
85,000	0.42	0.12	0.04	0.32	
75,000	0.36	0.10	0.04	0.24	
65,000	0.31	0.08	0.04	0.18	
55,000	0.19	0.07	0.04	0.15	
45,000	0.18	0.06	0.04	0.11	
35,000	0.15	0.05	0.04	0.10	
25,000	0.12	0.04	0.04	0.06	
20,000	0.08	~0.04	0.04	0.05	
15,000	0.07	~0.01	0.04	0.04	
10,000	0.06	0	0.04	~0.03	
5,000	0	0	0	0	No crack detectable

Table C.6
Stainless Steel 304
Crack Growth Data
Specimen I.D. SS16

$R_\varepsilon = 0$ $R_\gamma = -1$

$\frac{\Delta\varepsilon}{2} = 0$ $\frac{\Delta\gamma}{2} = 0.006$

N (Cycles)	L (mm)	a_1 (mm)	a_2 (mm)	a_3 (mm)	Comments
80,000	6.57	2.1	1.94	3.04	
70,000	---	0.53	1.88	----	Crack not completely on replica
60,000	2.87	0.45	1.88	0.67	
50,000	2.18	0	2.05	0.34	
40,000	2.06	0	2.02	0.18	
30,000	2.06	0	2.01	0.18	Crack branching occurs
20,000	~1.96	0	~1.96	0	
10,000	~1.96	0	~1.96	0	
5,000	~1.96	0	~1.96	0	

Table C.7
Stainless Steel 304
Crack Growth Data
Specimen I.D. SS09

$R_\varepsilon = 0$ $R_\gamma = -1$

$\frac{\Delta\varepsilon}{2} = 0$ $\frac{\Delta\gamma}{2} = 0.0035$

N (Cycles)	L (mm)	a_1 (mm)	a_2 (mm)	a_3 (mm)	Comments
1,000,000	2.25	1.09	~0	1.12	
900,000	1.08	~0.52	~0	~0.58	
800,000	0.65	0.28	~0	0.38	
700,000	0.36	0.14	~0	0.21	
600,000	0.18	0.04	~0	0.14	
500,000	0.14	~0.01	~0	0.14	
400,000	0.11	0	~0	0.11	
300,000	0.10	0	~0	0.10	
200,000	0.05	0	~0	0.05	No perceptible shear crack. Growth occurs at 45 degrees.
150,000	0	0	~0		No crack detectable.

Table C.8
Stainless Steel 304
Crack Growth Data
Specimen I.D. SS20

$R_\varepsilon = 0$ $R_\gamma = -1$

$\frac{\Delta\varepsilon}{2} = 0$ $\frac{\Delta\gamma}{2} = 0.0035$

N (Cycles)	L (mm)	a_1 (mm)	a_2 (mm)	a_3 (mm)	Comments
800,000	5.91	2.95	0.17	2.86	
750,000	2.34	1.07	0.17	1.19	
700,000	1.37	0.59	0.17	0.65	
650,000	0.99	0.41	0.17	0.43	
600,000	0.76	0.28	0.16	0.31	
550,000	0.59	0.20	0.16	0.25	
500,000	0.44	0.12	0.16	0.21	
450,000	0.32	0.09	0.16	0.15	a_1 appears
400,000	0.27	0	0.16	0.12	
350,000	0.22	0	0.16	0.11	
300,000	0.19	0	0.16	0.10	
250,000	0.17	0	0.16	0.07	
200,000	0.17	0	0.16	0.06	Crack branching occurs
150,000	0.16	0	0.16	0	
100,000	0.16	0	0.16	0	
50,000	0.16	0	0.16	0	
10,000	0.16	0	0.16	0	Crack grows from a stringer inclusion

Table C.9
Stainless Steel 316
Crack Growth Data
Specimen I.D. SJ03

$R_\varepsilon = 0$ $\qquad$ $R_\gamma = -1$

$\frac{\Delta\varepsilon}{2} = 0$ $\qquad$ $\frac{\Delta\gamma}{2} = 0.0173$

N (Cycles)	L (mm)	Comments
2100	10.29	Specimen fails in shear (No a_1 or a_3 cracks)
1800	7.35	
1500	5.48	Crack branches, but immediately returns to shear cracking
1200	5.05	
900	3.92	
600	3.59	
350	3.09	Cracks link up
50	0.89	

Table C.10
Stainless Steel 316
Crack Growth Data
Specimen I.D. SJ01

$R_\varepsilon = 0$ $R_\gamma = -1$

$\frac{\Delta\varepsilon}{2} = 0$ $\frac{\Delta\gamma}{2} = 0.008$

N (cycles)	L (mm)	a_1 (mm)	a_2 (mm)	a_3 (mm)	Comments
38,000	18.3	7.4	1.3	6.5	
35,000	3.04	1.11	1.24	0.92	
30,000	1.52	0.26	1.22	0.52	
25,000	1.32	0.09	1.22	0.22	Crack branching occurs
20,000	1.22	0	1.22	0	
15,000	1.02	0	1.02	0	Cracks link up (between 10 & 15 k)
10,000	0.39	0	0.39	0	
5,000	0.08	0	0.08	0	
1,000	0	0	0	0	No crack detectable

Table C.11
Stainless Steel 316
Crack Growth Data
Specimen I.D. SJ02

$R_\varepsilon = 0$ $R_\gamma = -1$

$\frac{\Delta\varepsilon}{2} = 0$ $\frac{\Delta\gamma}{2} = 0.006$

N (cycles)	L (mm)	a_1 (mm)	a_2 (mm)	a_3 (mm)	Comments
99,810	5.9	1.02	1.01	5.19	
90,000	1.76	0.69	0.98	0.36	
80,000	1.24	0.42	0.98	0.18	
70,000	1.14	0.19	0.97	0.08	
60,000	1.05	0.09	0.97	0.04	
50,000	1.02	0.05	0.97	0.03	
40,000	0.99	0.04	0.97	0	Cracks link up Crack branching occurs
30,000	0.71	0	0.71	0	
20,000	0.47	0	0.47	0	
10,000	0.35	0	0.35	0	
5,000	0.35	0	0.35	0	
0	0	0	0	0	

Table C.12
Stainless Steel 316
Crack Growth Data
Specimen I.D. SJ07

$R_\varepsilon = 0$ $R_\gamma = -1$

$\frac{\Delta\varepsilon}{2} = 0$ $\frac{\Delta\gamma}{2} = 0.006$

N (Cycles)	L (mm)	a_1 (mm)	a_2 (mm)	a_3 (mm)	Comments
114,730	11.13	3.69	9.20	--	
110,000	6.02	1.17	9.03	--	a_3 branch grows into another crack
100,000	4.77	0.17	4.06	1.15	
90,000	4.56	0.17	4.05	0.64	
80,000	4.20	0.17	4.05	0.35	
70,000	4.14	0.11	4.05	0.25	
60,000	4.13	0.11	4.05	0.21	
50,000	4.07	0.10	4.03	0.10	
40,000	4.02	0.05	4.02	0.08	
30,000	4.02	0.03	4.02	0.03	
20,000	3.94	0.02	3.94	0.03	Crack branching occurs
10,000	3.94	0	3.94	0	
5,000	3.10	0	3.10	0	

Table C.13
Stainless Steel 316
Crack Growth Data
Specimen I.D. SJ04

$R_\varepsilon = 0$ $\qquad$ $R_\gamma = -1$

$\frac{\Delta\varepsilon}{2} = 0$ $\qquad$ $\frac{\Delta\gamma}{2} = 0.0035$

N (Cycles	L (mm)	a_1 (mm)	a_2 (mm)	a_3 (mm)	Comments
585,000	12.10	4.70	1.59	6.13	
560,000	4.81	1.23	1.53	2.30	
480,000	2.35	0.51	1.53	0.51	
400,000	1.86	0.26	1.50	0.27	
320,000	1.67	0.09	1.50	0.13	
240,000	1.57	0.07	1.50	0.08	
160,000	1.54	0.04	1.50	0	Crack branching occurs
80,000	1.48	0	1.48	0	
48,000	1.45	0	1.45	0	Cracks link up
40,000	0.64	0	0.64	0	
32,000	0.61	0	0.61	0	
24,000	0.59	0	0.59	0	
16,000	0.53	0	0.53	0	Cracks link up
8,000	0.15	0	0.15	0	

Table C.14
Stainless Steel 316
Crack Growth Data
Specimen I.D. SJ08

$R_\varepsilon = 0$ $R_\gamma = -1$

$\frac{\Delta\varepsilon}{2} = 0$ $\frac{\Delta\gamma}{2} = 0.0035$

N (Cycles)	L (mm)	a_1 (mm)	a_2 (mm)	a_3 (mm)	Comments
1,024,000	27.43	13.30	0.12	14.70	
1,000,000	5.06	2.35	0.12	2.57	
950,000	2.43	1.19	0.12	1.16	
900,000	1.73	0.84	0.12	0.76	
850,000	0.13	0.57	0.12	0.44	
800,000	0.91	0.45	0.12	0.34	
750,000	0.73	0.34	0.12	0.27	
700,000	0.52	0.25	0.12	0.24	
650,000	0.49	0.21	0.12	0.22	
600,000	0.45	0.19	0.12	0.15	
550,000	0.45	0.12	0.12	0.11	
500,000	0.32	0.11	0.12	0.09	
463,140	0.29	0.10	0.12	0.07	
450,000	0.27	0.09	0.12	0.05	
400,000	0.25	0.07	0.12	0.05	
350,000	0.23	0.06	0.12	0.05	
250,000	-0.14	-0.01	0.12	0	Crack branching occurs
200,000	0.12	0	0	0	
150,000	0.12	0	0	0	
100,000	0.09	0	0	0	
50,000	0.08	0	0	0	
10,000	0.08	0	0	0	

Table C.15
Stainless Steel 316
Crack Growth Data
Specimen I.D. SJ06

$R_\varepsilon = 0$ $\qquad$ $R_\gamma = -1$

$\frac{\Delta\varepsilon}{2} = 0$ $\qquad$ $\frac{\Delta\gamma}{2} = 0.003$

N (Cycles)	L (mm)	a_1 (mm)	a_2 (mm)	a_3 (mm)	Comments
900,000	13.9	6.09	1.29	6.34	
850,000	3.79	1.27	1.24	1.49	
783,000	2.64	0.72	1.28	0.82	
750,000	2.28	0.60	1.25	0.65	
700,000	2.31	0.59	1.25	0.64	
650,000	1.86	0.37	1.25	0.41	
600,000	1.70	0.26	1.25	0.30	
550,000	1.47	0.22	1.25	0.24	
500,000	1.55	0.19	1.25	0.14	
450,000	1.43	0.18	1.25	0.09	
400,000	1.37	0.10	1.25	0.07	
350,000	1.30	0.04	1.25	0.04	
300,000	1.28	0.04	1.25	0	Crack branching occurs
250,000	1.24	0	1.24	0	
200,000	1.21	0	1.21	0	
150,000	1.20	0	1.20	0	
50,000	1.10	0	1.10	0	
25,000	0.53	0	0.53	0	

APPENDIX D: CRACK GROWTH PLOTS

Page

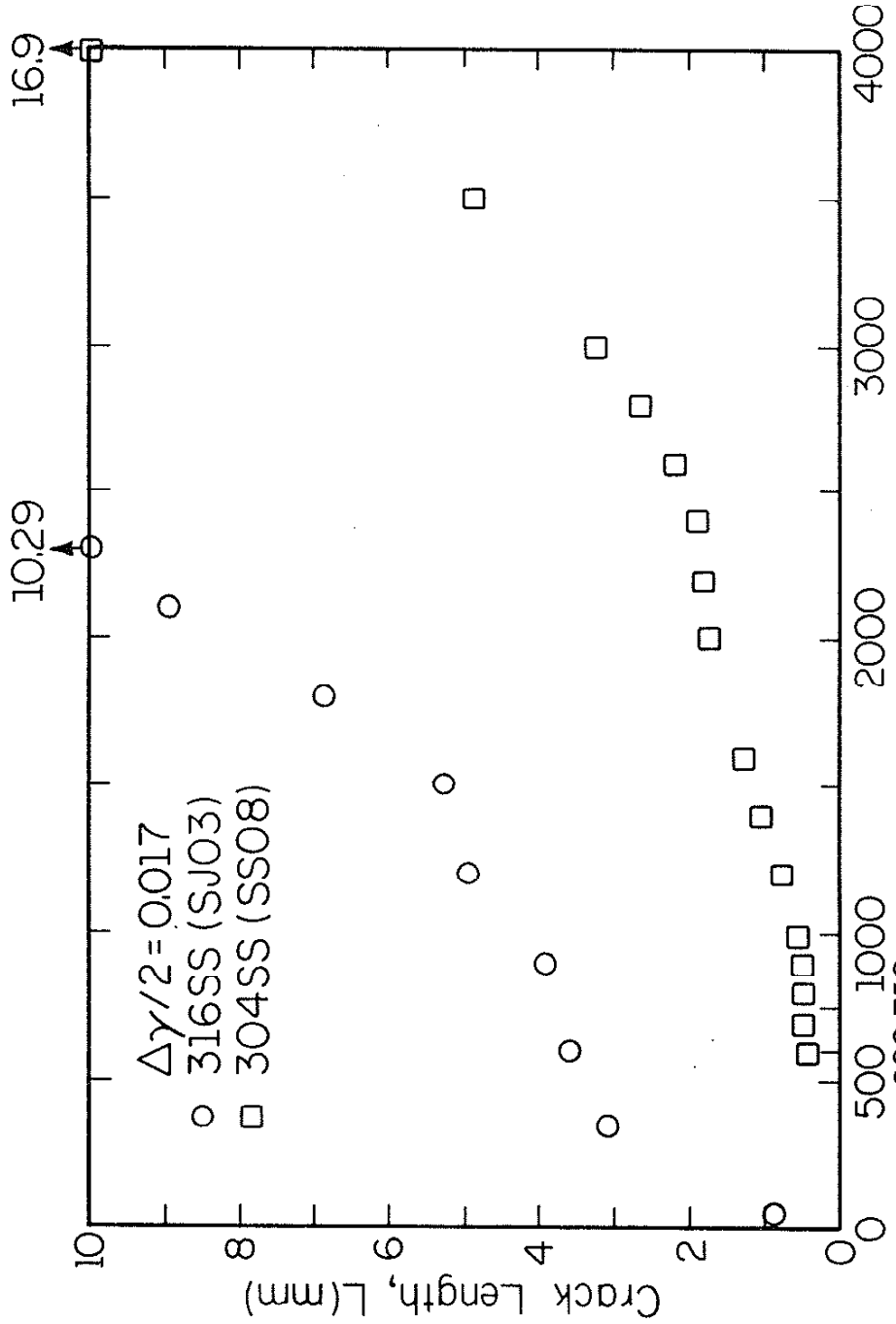

Figure D.1 $\frac{\Delta\gamma}{2} = 0.0173$

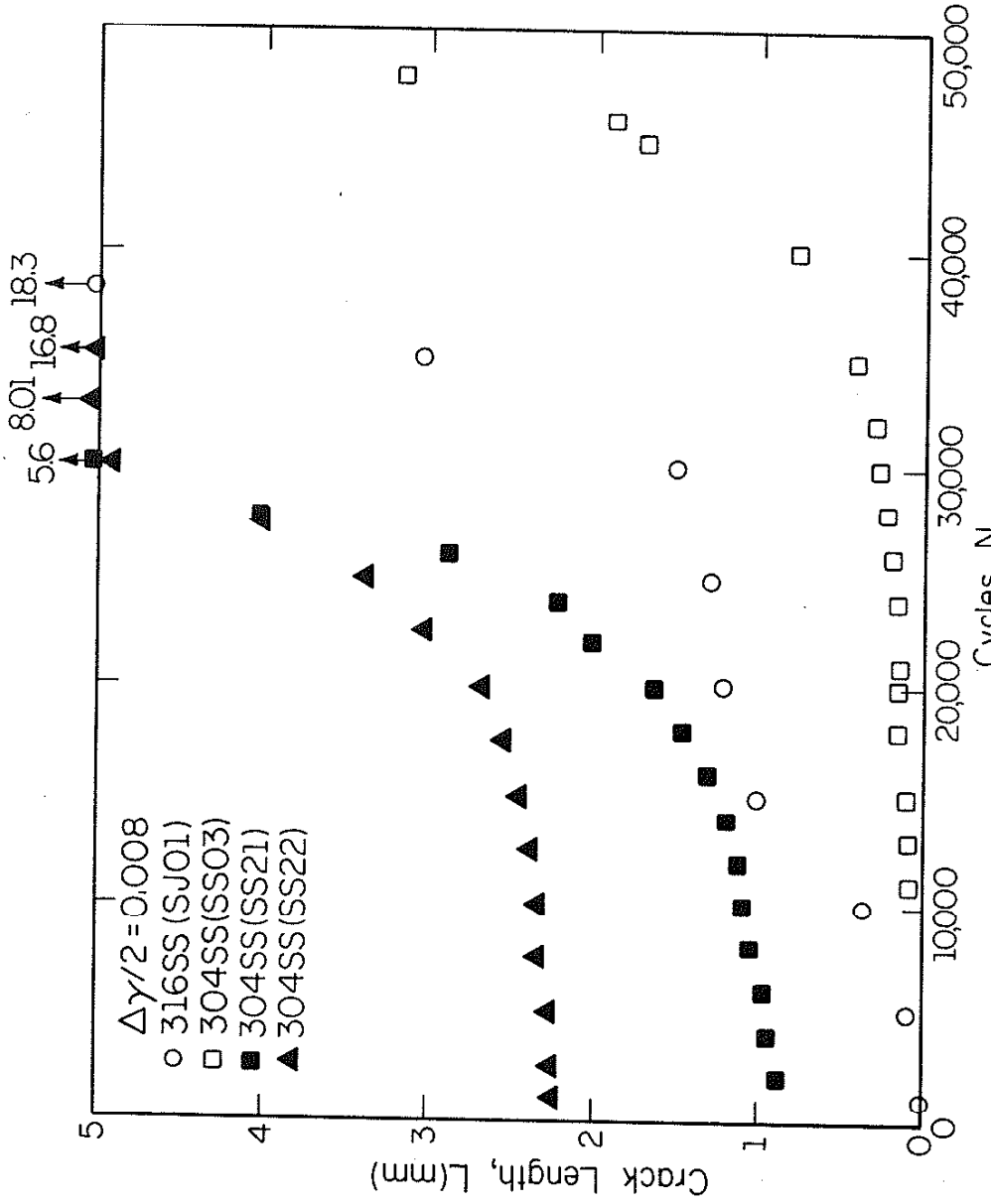

Figure D.2 $\frac{\Delta\gamma}{2} = 0.008$

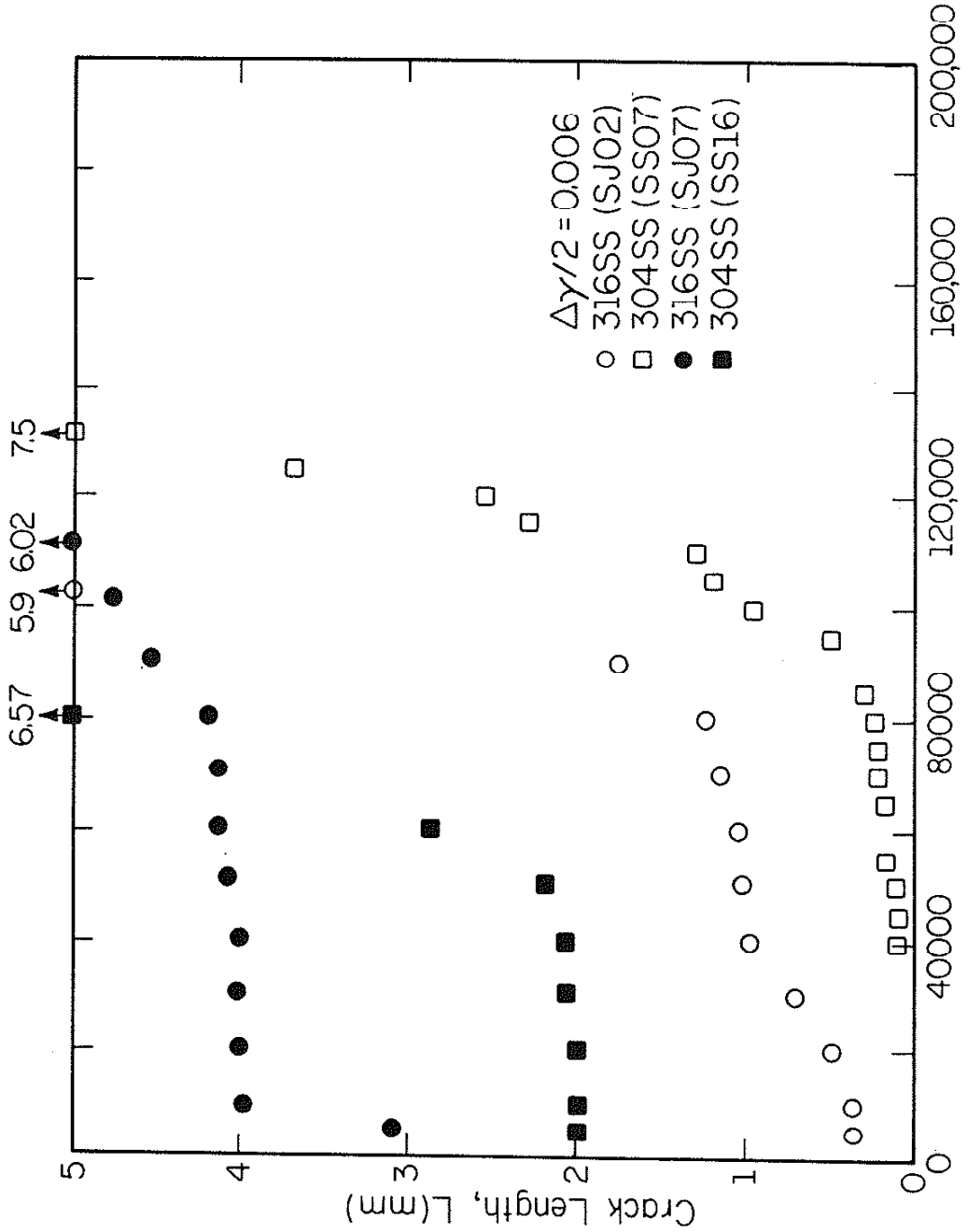

Figure D.3 $\frac{\Delta\gamma}{2} = 0.006$

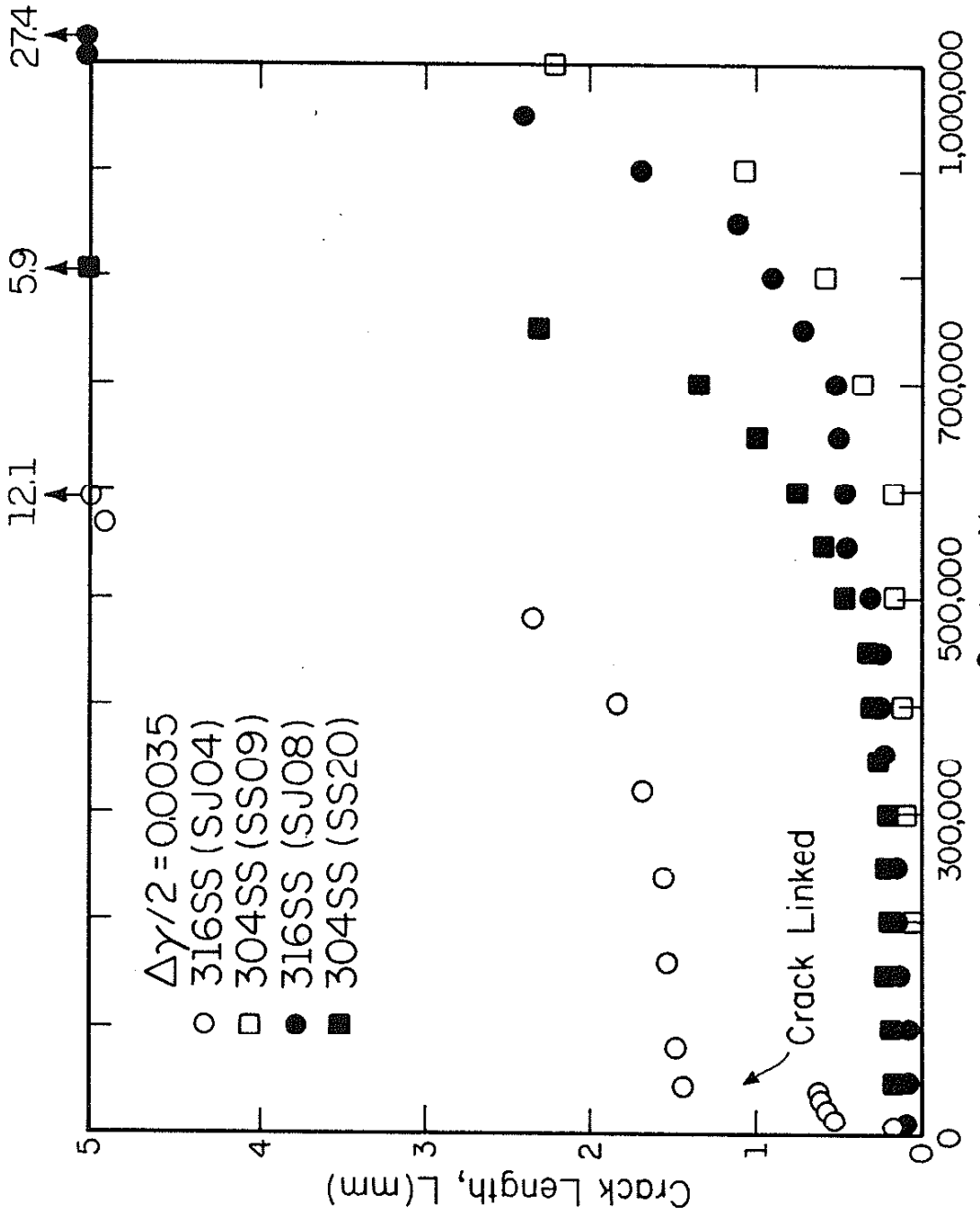

Figure D.4 $\frac{\Delta\gamma}{2} = 0.0035$

REFERENCES

1. Ewing, J. A., and Humfrey, J. C., "Fracture of Metals Under Repeated Alternations of Stress," Philosophical Transactions of the Royal Society of London, Vol. 200, Series A, 1903, pp. 241-253.

2. Fine, M. E., Ritchie, R. O., "Fatigue-Crack Initiation and Near-Threshold Crack Growth," Fatigue and Microstructure, ASM Materials Science Seminar, St. Louis, Mo., 1978, pp. 245-278.

3. Laird, Campbell, "Mechanisms and Theories of Fatigue," Fatigue and Microstructure, ASM Materials Science Seminar, St. Louis, MO., 1978, pp. 149-203.

4. Mughrabi, H., "Dislocations in Fatigue," Presented at the 50th anniversary meeting on "Dislocations and Properties of Real Materials," at the Royal Society, London, Dec. 11-12, 1984, and to be published in the conference proceedings by the Metal Society, London.

5. Laird, C., "The Application of Dislocation Concepts in Fatigue," in Dislocations in Solids, Ed. by F. R. N. Nabarro, North-Holland Publishing Co., 1983.

6. Boettner, R. C., Laird, C., and McEvily, A. J., "Crack Nucleation and Growth in High Strain-Low Cycle Fatigue," Trans. of Metallurgical Society of AIME, Vol. 233, 1965, pp. 379-387.

7. Frost, N. E., Marsh, K. J., and Pook, L. P., Metal Fatigue, Oxford University Press, 1974.

8. Tipnis, V. A., and Cook, N. H., "The Influence of Stress-State and Inclusion Content on Ductile Fracture with Rotation," J. of Basic Engineering, Trans. of American Society of Mechanical Engineers, Series D, September 1967, pp. 533-540.

9. Stanzl, S. E., "Fatigue Crack Growth (Physical Principles, Models and Experimental Results)," Res. Mechanica, Vol. 5, 1982, pp. 241-292.

10. Gough, H. J., "Crystalline Structure in Relation to Failure of Metals - Especially by Fatigue," Edgar Marburg Lecture, Proc. ASTM 33, Part II, 1933, pp. 3-114.

11. Forsyth, P. J. E., "A Two Stage Process of Fatigue Crack Growth," Proceedings of the Symposium on Crack Propagation, Cranfield, England, 1961, pp. 76-94.

12. Parsons, M. W., and Pascoe, K. J., "Observations of Surface Deformation, Crack Initiation and Crack Growth in Low-Cycle Fatigue Under Biaxial Stress," Materials Science and Engineering, Vol. 22, 1976, pp. 31-50.